UCRL-19397

c.2

A MEASUREMENT OF THE BRANCHING RATIO $K_L^o \to 2\pi^o / K_L^o \to 3\pi^o$

William P. Oliver
(Ph.D. Thesis)

November 1969

AEC Contract No. W-7405-eng-48

LAWRENCE RADIATION LABORATORY
UNIVERSITY of CALIFORNIA BERKELEY

UCRL-19397

DISCLAIMER

A MEASUREMENT OF THE BRANCHING RATIO $K_L^o \to 2\pi^o / K_L^o \to 3\pi^o$

Contents

A MEASUREMENT OF THE BRANCHING RATIO $K_L^o \to 2\pi^o / K_L^o \to 3\pi^o$

Lawrence Radiation Laboratory
University of California
Berkeley, California

ABSTRACT

The rate of the decay $K_L^o \to 2\pi^o$ has been measured relative to that of $K_L^o \to 3\pi^o$ using a monoenergetic K_L^o beam and a nearly 4π solid-angle detection system of lead-plate spark chambers and shower counters. The analysis of the fraction (40%) of the data at the Lawrence Radiation Laboratory gives for the branching ratio 0.0100 ± 0.0018 (statistical) ± 0.0009 (systematic). This result leads to a value for the branching ratio $\frac{\Gamma(K_L \to 2\pi^o)}{\Gamma(K_L \to \pi^+\pi^-)}$ of $1.37 \pm .25$ (statistical) $\pm$ .14 (systematic). The significant difference between this ratio and the ratio $\frac{\Gamma(K_S \to 2\pi^o)}{\Gamma(K_S \to \pi^+\pi^-)}$ implies that CP violation must occur at least in part in the $K^o \to 2\pi$ decay process itself.

I. INTRODUCTION

The K^o meson, and its antiparticle the $\bar{K}^o$, are produced in strong interactions in states of definite energy with strangeness eigenvalues +1 for the K^o and -1 for the $\bar{K}^o$. Since strong interactions are invariant under charge conjugation, the K^o and $\bar{K}^o$ states are degenerate in energy.

The K^o and $\bar{K}^o$ are unstable under strangeness-changing weak interactions. The states K^o and $\bar{K}^o$ do not decay in simple exponential fashion because of the possibility of transitions between the two states by processes such as $K^o \to \pi^+\pi^- \to \bar{K}^o$. The time-evolution of two degenerate unstable states is a complicated problem in quantum mechanics. Detailed approximate treatments have been presented by Kabir,[1] Terentev,[2] and others. These treatments are based in part on earlier formulations given by Weisskopf and Wigner[3] and Breit and Lowen.[4]

The result of these treatments is that the free particle K^o- $\bar{K}^o$ system develops in time (in the Wigner-Weisskopf approximation) according to the equation[5]

$$i\frac{d\psi(t)}{dt} = (M - i\Gamma)\psi(t) \tag{1}$$

where

$$\psi(t) = a(t)|K^o> + b(t)|\bar{K}^o> = \begin{vmatrix} a(t) \\ b(t) \end{vmatrix} .$$

The elements of the (2×2) matrices Γ and M are (neglecting terms of third order in H_{wk})

$$\Gamma_{11} = \pi\sum_F \rho_F |<F|H_{wk}|\ K^o>|^2$$

$$\Gamma_{22} = \pi \sum_F \rho_F |<F|H_{wk}|\bar{K}^o>|^2$$

$$\Gamma_{12}^* = \Gamma_{21} = \pi \sum_F \rho_F <\bar{K}^o|H_{wk}|\ F><F\ |H_{wk}|\ K^o>$$

$$M_{11} = m_{K^o} + \langle K^o | H_{wk} | K^o \rangle + P \sum_n \frac{|\langle n | H_{wk} | K^o \rangle|^2}{m_{K^o} - E_n}$$

$$M_{22} = m_{K^o} + \langle \bar{K}^o | H_{wk} | \bar{K}^o \rangle + P \sum_n \frac{|\langle n | H_{wk} | \bar{K}^o \rangle|^2}{m_{K^o} - E_n}$$

$$M_{12}^* = M_{21} = \langle \bar{K}^o | H_{wk} | K^o \rangle + P \sum_n \frac{\langle \bar{K}^o | H_{wk} | n \rangle \langle n | H_{wk} | K^o \rangle}{m_{K^o} - E_n}$$

where H_{wk} is the weak-interaction Hamiltonian, $|n\rangle$ are eigenstates of the strong-interaction Hamiltonian, $|F\rangle$ are physical decay states and ρ_F are the densities of final states per unit energy. The sum over all eigenstates of the strong-interaction Hamiltonian has been formally divided into two terms. The principal value P denotes the contribution of states for which $E_n \neq m_{K^o}$. The states for which $E_n = m_{K^o}$ are the physical decay states $|F\rangle$. The contribution of these states is represented by the Γ matrix.

It is always possible to find two linear combinations of the $|K^o\rangle$ and $|\bar{K}^o\rangle$ states which uncouple the differential equations in Eq. (1). These two linear combinations correspond to particles with definite masses and lifetimes. The state with the longer lifetime is the K_L^o; the other is the K_S^o.

Invariance of H_{wk} under the combined operation of charge conjugation and space inversion would require that $M - i\Gamma$ be symmetric and have equal diagonal elements. The states which then uncouple Eq. (1) are eigenstates of CP. The amplitudes for K^o decay into 2π final states are much larger than the amplitudes for decay into the other possible final states. Since the 2π state is a CP-even eigenstate, the K_S^o and K_L^o would be identified as the CP-even and CP-odd eigenstates respectively. If CP were conserved,

the K_L^o and K_S^o would be expected to have greatly different lifetimes since the highly-favored 2π states are available only to the K_S^o. The K_L^o lifetime is in fact 600 times longer than the K_S lifetime, indicating that CP must be at least a nearly conserved quantity in the $K^o \to 2\pi$ decay process.

In 1964 it was discovered that the K_L^o decays into $\pi^+\pi^-$ in apparent violation of CP invariance.[6] Attempts were made to explain away this effect while retaining CP invariance in the interactions of known elementary particles. The apparent $K_L^o \to \pi^+\pi^-$ decays might be the result of a cascade process such as

$$K_L^o \to S + K_S^o \quad (K_S^o \to \pi^+\pi^-)$$

where S is a new particle with mass less than the $K_L^o - K_S^o$ mass difference.[7] There also might exist a field of cosmological origin in which the K^o and $\bar{K}^o$ have different potential energies. The external field would alter the relative phase between the K^o and $\bar{K}^o$ in the K_L^o state and thereby generate an admixture of the K_S^o state which then decays CP-invariantly into $\pi^+\pi^-$.

An experiment in which maximal constructive interference was found between the processes $K_L^o \to \pi^+\pi^-$ and regenerated $K_S^o \to \pi^+\pi^-$ offered strong evidence against both these hypotheses.[8] The fact that interference occurred at all invalidates the cascade hypothesis. The amplitudes for the process $K_L^o \to S + K_S^o \quad (K_S^o \to \pi^+\pi^-)$ have no constant phase relation to the amplitudes for regenerated $K_S^o \to \pi^+\pi^-$ decays so there should be no observable interference effects. A field of cosmological origin would be expected to generate a K_S^o state approximately 90 deg out of phase with

the K_S^o state generated by the differential absorption of K^o and $\bar{K}^o$ in nuclear matter.[1] The interference between $K_L^o \to \pi^+\pi^-$ and regenerated $K_S^o \to \pi^+\pi^-$ should therefore be minimal, contrary to what was observed. The cosmological hypothesis also predicts in general a dependence on energy of the $K_L^o \to \pi^+\pi^-$ branching ratio. No such energy dependence has been observed.[6,9,10]

If the occurrence of $K_L^o \to 2\pi$ decays is taken to mean that the interactions of known elementary particles are not CP invariant, it still remains to be determined exactly which processes are the carriers of the CP violation. If CP is violated only in a process which does not connect the K^o or $\bar{K}^o$ to a physically realizable decay channel, the only observable effects will be through the mixing of CP eigenstates in the K_L^o and K_S^o states. (An example of this type of process occurs in the theory of Wolfenstein in which CP violation occurs only in the first-order $K^o \underset{\leftarrow}{\rightarrow} \bar{K}^o$ transitions induced by a new, $\Delta S = 2$, superweak interaction.) Each CP component of the K_L^o and K_S^o states then decays CP-invariantly into physical decay channels. In particular, the ratios

$$R_L = \frac{\Gamma(K_L^o \to \pi^o\pi^o)}{\Gamma(K_L^o \to \pi^+\pi^-)} \quad \text{and} \quad R_S = \frac{\Gamma(K_S^o \to \pi^o\pi^o)}{\Gamma(K_S^o \to \pi^+\pi^-)}$$

will be equal.

Observation of an inequality of R_L and R_S eliminates the possibility that the superweak interaction is the sole carrier of CP violation and directly implies that CP is violated in the $K^o \to 2\pi$ decay process itself. Also, explanations of apparent CP-violation effects by means of new fields of cosmological origin or by presently unknown decay processes are eliminated since in both these cases the 2π final states stem from K_S^o states.

Measurements of the rate of $K_L^o \to 2\pi^o$ relative to the rate of

$K_L^o \to 3\pi^o$ have been made.[11-13] These measurements yield values of R_L which are consistent with equality of R_L and R_S. However a measurement of the $K_L^o \to 2\pi^o$ rate relative to the rate of regenerated $K_S^o \to 2\pi^o$ decays in carbon yields a value for R_L which differs by three standard deviations from R_S.[14]

II. EXPERIMENTAL APPARATUS

A. General Procedure

The purpose of the experiment was to measure the rate of the decay $K_L^o \to 2\pi^o$ relative to the rate of the decay $K_L^o \to 3\pi^o$. The design and arrangement of the experimental apparatus was such as to produce approximately monoenergetic K_L^o mesons which decayed in flight within a nearly 4π solid-angle gamma ray detection system. The layout of the experimental apparatus is shown in Fig. 1.

To create K_L^o mesons of known energy, a π^- beam was extracted from the Bevatron, momentum analyzed, and then directed to a 1.2-m long, liquid hydrogen target. The momentum spectrum of the π^- beam was chosen to maximize K^o production from the reaction $\pi^- p \to \Lambda^o K^o$ consistent with a contamination level of K^o's from the reaction $\pi^- p \to \Sigma^o K^o$ of only a few percent. The beam pions and charged particle background produced in the hydrogen target were swept to the side by two bending magnets. A neutral beam of forward-going neutrons, K^o's, and gamma rays was thereby created. The gamma rays were filtered from the neutral beam by 4-in. of lead placed about 5 ft downstream from the hydrogen target.

After the lead filter the remaining K^o's and neutrons drifted downstream a distance of 5 m where they entered a 1 m^3 air-filled decay volume which was enclosed by a five-sided cube of lead-plate spark chambers. The geometry for detecting gamma rays was enhanced by placing a tunnel consisting of lead-Lucite Cerenkov counters at the entrance to the spark chamber array.

Gamma rays from the decay in flight of a K_L^o meson into neutral pions were detected by two banks of scintillator-Cerenkov-trigger counters placed in the downstream spark chamber. The requirements of two gamma

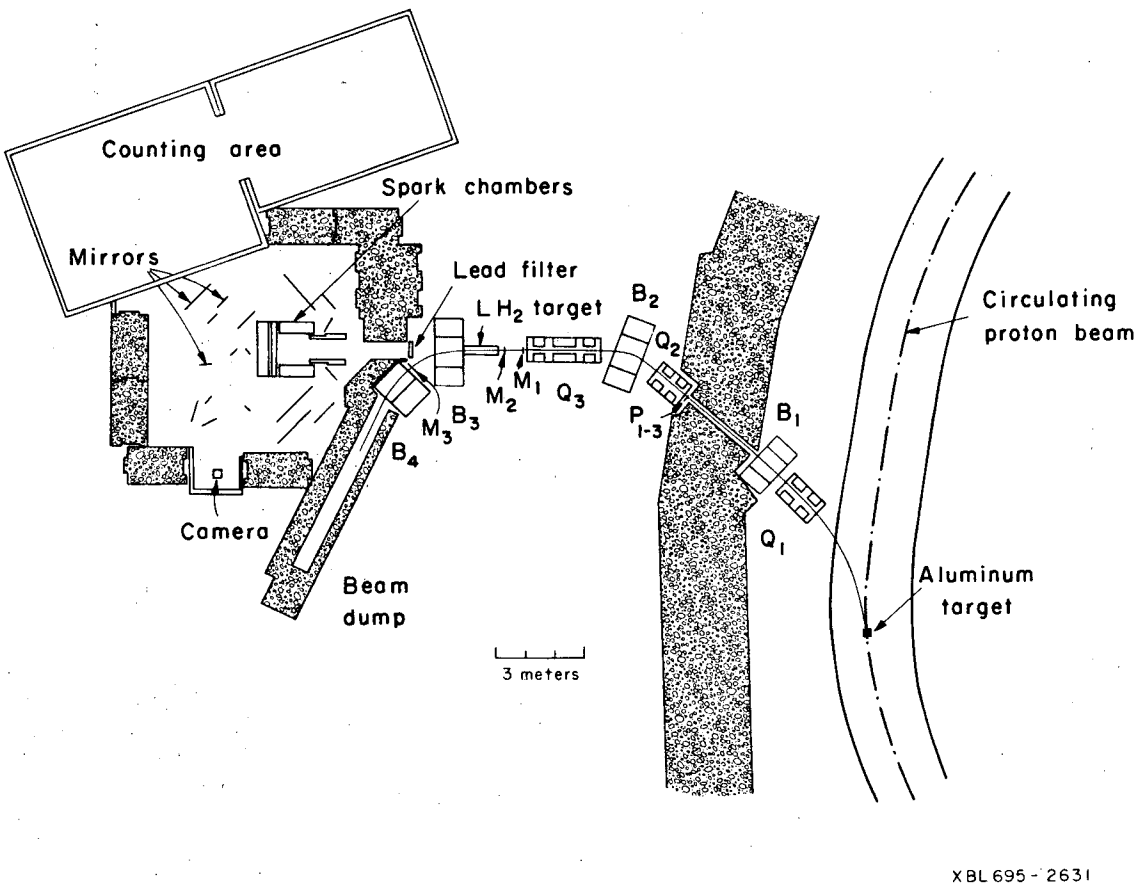

Fig. 1. Plan view of experiment.

ray showers in the downstream spark chamber separated by a minimum distance of 11-in., a π^- meson entering the liquid hydrogen target and not continuing along the beam, no charged particles detected in the lead filter, and no charged particles entering the spark chambers constituted the signature for a K_L^o decay into a neutral final state. The separation requirement for the trigger counters was used to discriminate against neutron interactions in the downstream spark chamber. 464 000 pictures were taken under this mode of operation. The total number of K_L^o neutral decays occurring within the fiducial volume was 20 000.

The detection efficiencies for $2\pi^o$ and $3\pi^o$ final states were approximately equal. Hence nearly all of the events detected were $3\pi^o$ decays. This large number of events served as a normalization for the rate of occurrence of $2\pi^o$ decays. The principal separation of $2\pi^o$ from $3\pi^o$ decays was accomplished by simply detecting five or six gamma ray showers in the spark chamber-tunnel shower counter complex. The remaining separation was carried out by determining if the observed directions and energies of the gamma rays were consistent with the kinematical constraints of the decay through an intermediate two-pion state of a K_L^o of momentum within the known range for the experiment.

The response of the spark chambers to gamma rays of known energy was determined by making calibration runs on $K_L^o \rightarrow \pi^+\pi^-\pi^o$. The 180 000 pictures taken with the charged signature yielded 1000 $K_L^o \rightarrow \pi^+\pi^-\pi^o$ decays and 4000 leptonic decays. The calibration runs were distributed frequently and uniformly throughout the entire run.

B. Beam

Pions for the beam were produced by bombarding a 10 by 1/4 by 1/2-in. aluminum target with 5.6 GeV protons of the internal circulating beam of the Bevatron. Aluminum was chosen as the target material to maximize the production of pions. Maximization of the pion flux required the use of a rather long target. To keep the apparent size of the pion source small it was necessary for the beam-transport system to accept pions produced in the forward direction in the target. The target location was varied by small amounts until a maximum in the electron contamination was reached indicating that the target was being viewed head-on. The electron contamination is expected to peak in the forward direction since gamma rays produced at an angle to the target escape more readily from the aluminum without conversion into electron-position pairs. The electrons were monitored by a 1 atm, 3-ft long, Freon 12-filled, gas Cerenkov counter which could be placed in the beam upstream of the liquid hydrogen target.

A flux of 5×10^{11} protons incident on the Al target produced a flux of 8×10^{6} pions, 2.6×10^{6} electrons, and 1.4×10^{6} muons in the momentum range 980±40 MeV/c (FWHM) incident on the liquid hydrogen target. The composition of the beam was determined by means of a high pressure (0 to 300 psi), Freon 13-filled, gas Cerenkov counter.

The elements of the beam transport system were:

Q_1 - 12-in. bore, 16, 16-in. long quadrupole doublet.

B_1 - 18-in. wide by 36-in. long H magnet with a 12-in. gap.

Q_2 - 12-in. bore, 16, 16-in. long quadrupole doublet.

B_2 - 18-in. wide by 36-in. long H magnet with an 8-in. gap.

Q_3 - 8-in. bore, 16, 32, 16-in. long quadrupole triplet.

B_3 - 18-in. wide by 36-in. long H magnet with a 20-in. gap.

B_4 - 16-in. wide by 36-in. long C magnet with an 8-in. gap.

Quadrupole Q_1 produced a focus of the target at the entrance to Q_2. The dispersion due to the Bevatron field and the field of magnet B_1 spread the foci for the various momenta horizontally across the entrance to Q_2. Here the final momentum selection was made by inserting an 11 1/2-in. diameter lead collimator into Q_2. Q_2 served as a field lens, recombining the momentum foci at its entrance to a single focus at the hydrogen target. To shield the hydrogen target from degraded particles resulting from collisions of the beam with the momentum-defining collimator, a second bend in the beam of 40 deg was made by magnet B_2. Quadrupole Q_3 then focused the image of the Al target at the entrance of Q_2 on the liquid hydrogen target. Magnets B_3 and B_4 were the sweeping magnets used to create the neutral beam which drifted downstream into the spark chamber array.

Magnet B_3 was also used as an analyzer in a measurement of the momentum distribution of the beam. The trajectories in the beam at the exit of quadrupole Q_3 were sampled by two sets of ten 0.32-cm wide by 0.635-cm thick by 20.3-cm high finger counters. In the first set the finger counters were spaced at 2-cm intervals and in the second at 2.5-cm intervals. The first set was situated at the exit of Q_3 and the second was situated at the entrance to magnet B_3. The beam was extensively sampled by taking data for nine different orientations of the sets obtained by translating each set independently $\pm$ 1/3 of an interval. Trajectories through B_3 were determined with the aid of an additional 0.32-cm wide by 0.635-cm thick by 20.3-cm long finger counter at the normal beam center 0.9-m downstream from the end of B_3. The momentum spectrum for beam particles traversing all possible pairs of the first two sets was then

determined by measuring all triples rates as a function of B_3 current. The triples rates were normalized to a monitor that covered the entire beam. The momentum values for the finger counter triplets at each B_3 current were determined by wire orbit techniques. The momentum resolution of a triplet was about 1%. The result of the momentum measurement is shown in Fig. 2.

The K_L^o momentum distribution was calculated by Monte Carlo techniques using the known cross sections for K^o production.[15-16] The effect of ionization energy loss by the pions in the liquid hydrogen was taken into account. The momentum variation of the absorption of pions in the hydrogen and of K_L^o's in both the hydrogen and the lead filter was assumed to have a negligible effect on the shape of the momentum spectrum of the K_L^o beam. The variation in survival against decay for K_L^o's of different momentum was included to calculate the momentum distribution of the K_L^o beam at the entrance to the spark chamber array. This distribution is shown in Fig. 3. A flux of 8×10^6 pions incident on the hydrogen target was calculated to produce 40 K_L^o's traversing the decay volume.

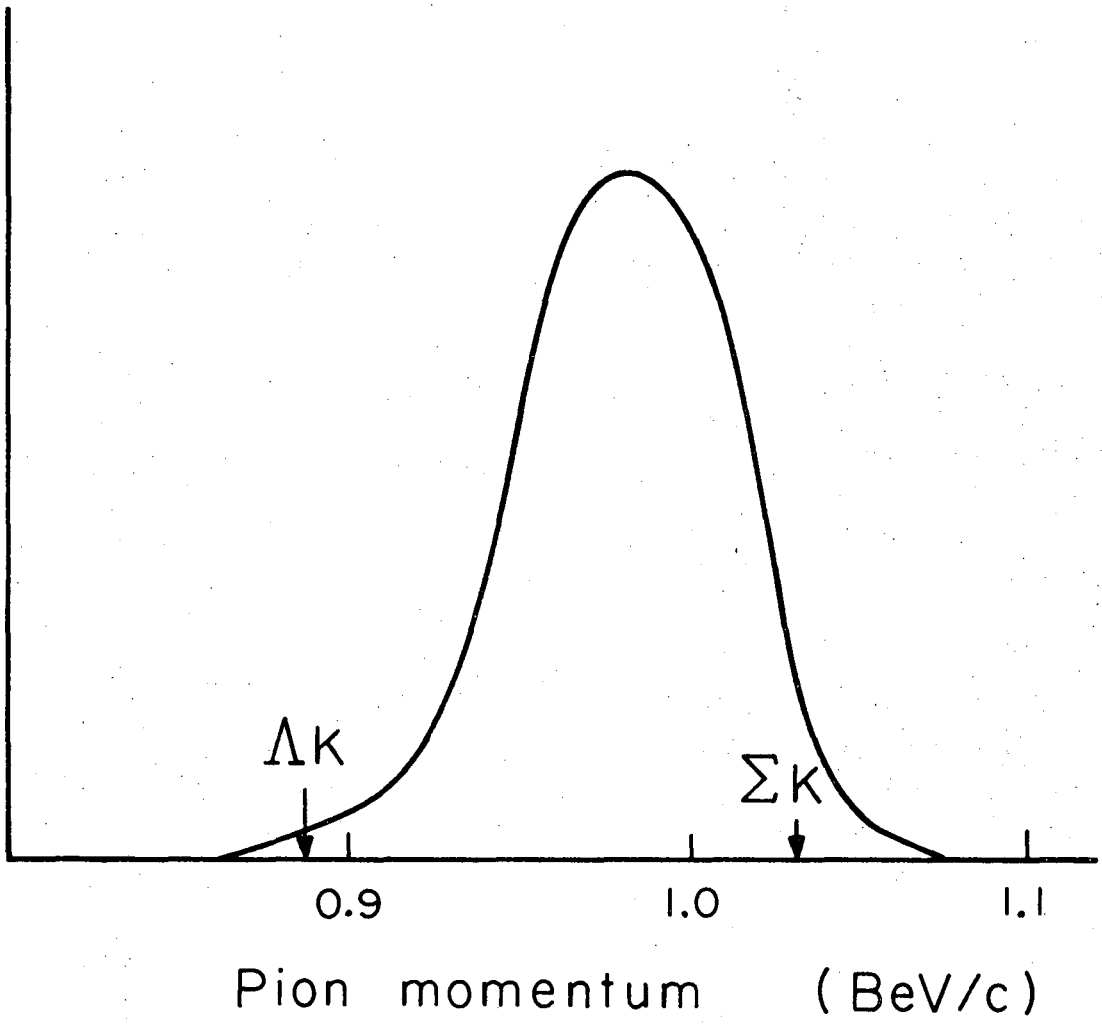

XBL695-2632

Fig. 2. Measured momentum distribution of the π^- beam at the hydrogen target. Thresholds for Λ^o and Σ^o production are shown.

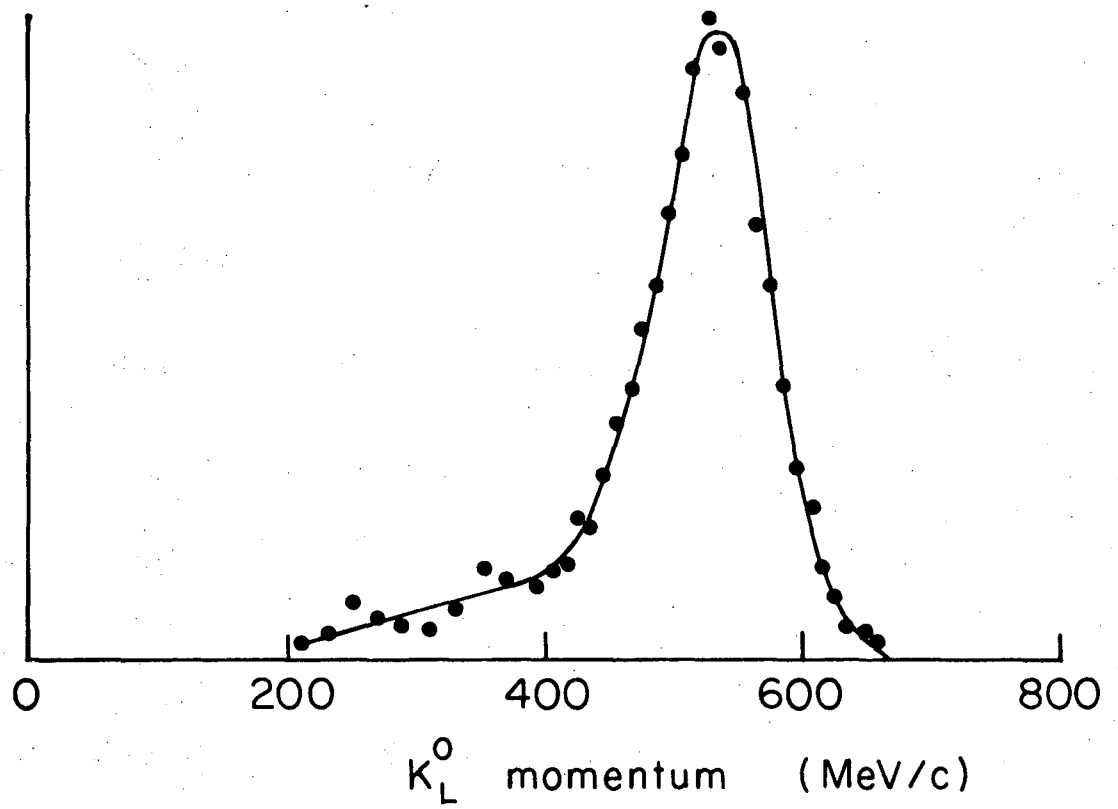

XBL695-2662

Fig. 3. Calculated momentum distribution of the K_L^0 beam at the entrance to the spark chamber array. The points are the results of the Monte Carlo calculation.

C. Gamma Ray Detectors

The 1 m^3 decay volume was surrounded on five sides by lead-plate spark chambers. The upstream side was left open for the entering K_L^o mesons. The decay volume was further enclosed by placing a gamma shower counter which had the geometry of a four-sided tunnel at the entrance to the spark chamber array. The total solid angle subtended by the gamma detection assembly was about 98% in the K_L^o barycentric system.

The spark chambers were assembled in modular form. The first module in each chamber was constructed with five 0.048-in. Al plates to provide identification of charged particles entering the spark chamber. The spark chambers were then filled out with modules constructed with lead plates. Each lead plate was 0.032-in. thick and was stiffened by gluing 0.016-in. thick Al plates to each side. Six lead plates followed by one Al plate then formed one six-gap lead module. Each lead module had a total thickness of 2 5/16-in. and contained 0.915 radiation lengths of lead. The plates were glued to Lucite frames to form gaps of 5/16-in. The gap spacing was maintained by gluing 1/4 by 1/4 by 5/16-in. Lucite blocks between the plates at intervals of 8 in. The faces of these blocks were polished and accurately parallel permitting photographing of sparks anywhere in the active volume.

The four lateral spark chambers were 4 by 5-ft and consisted of one Al module followed by seven lead modules. The downstream chamber was 6 1/2 by 6 1/2-ft but was electrically two different chambers. A 1-in. wide Lucite bar running vertically separated the chamber into two halves: one half was 3 1/2 by 6 1/2-ft and the other was 3 by 6 1/2-ft. The position of the Lucite bar was staggered for the different modules. The chamber consisted of one Al module followed by eight lead modules.

The entrance tunnel to the spark chamber array contained an independent shower counter in each of its four sides. Each counter was 4-ft long in the beam direction and 3-ft wide. The counters were 5.7-radiation lengths thick for the downstream 2-ft length and widened to 8.5-radiation lengths for the upstream 2-ft length. The shower counter configuration is shown in Fig. 4. The tunnel extended 6 in. into the region enclosed by the spark chambers. The counters were constructed by interleaving sheets of 1/32-in. lead and 1/8-in. Lucite. The sheets of lead and Lucite were preceded by a 1/4-in. sheet of scintillator. The Cerenkov light generated in the Lucite was viewed by a battery of six 58 AVP phototubes situated along the upstream edge of the counter. The outputs of the six tubes were added to form a single output for each of the four counters.

Showers from neutral decays were detected by two banks of trigger counters placed in the downstream spark chamber. Each bank consisted of 11 counters stacked vertically. The trigger counters were 5 1/2-in. wide and 5-ft long. The first bank of counters was placed after the first lead module and the second bank after the second module. Each trigger counter was a scintillator-Cerenkov pair. The Cerenkov member was a Lucite slab 1 1/2-in. thick. The efficiency for detecting a single highly relativistic particle at perpendicular incidence was measured to be 95 to 97% and was uniform to within 2% over the entire length. The two Cerenkov radiators at the same height in the two banks were combined optically at a 58 AVP phototube. The corresponding scintillators were viewed separately by two 56 AVP phototubes and the two signals were added passively at the bases.

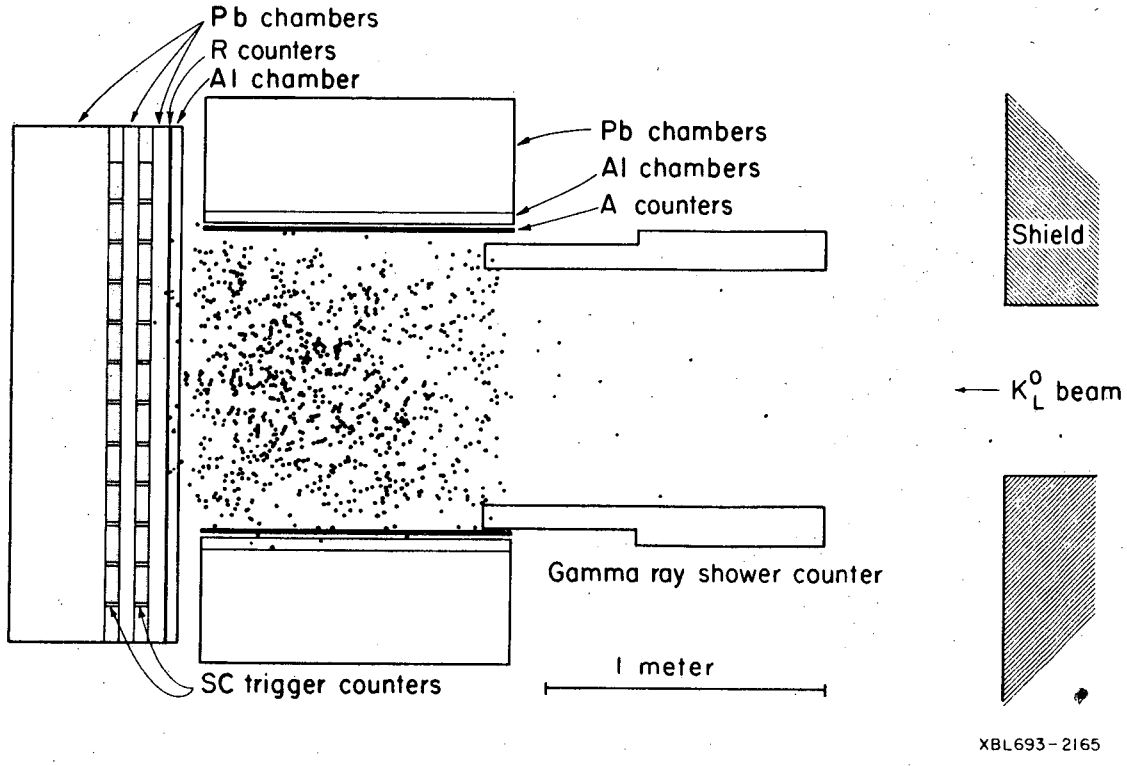

Fig. 4. Vertical section through gamma detector assembly. Vertices of all four-shower events having no counts in the gamma ray shower counter are projected on this plane. $2\pi^0$ events have a similar distribution. The fiducial volume boundaries are 5 cm from the chambers.

D. Optical System

Two orthogonal views of each spark chamber were combined into one frame by a system of 46 front-surfaced mirrors. The ten views were arranged on the film in three groups. Each group corresponded to a possible real-space view of the spark chamber array. The correspondence between the views on the film and views in real space is shown in Fig. 5. Within each view the geometrical relationship between the chambers was nearly the same on the film as it was in real space. This arrangement made it possible to count accurately the number of showers present in an event at the scanning stage of the analysis. The cases in which a shower passed through more than one chamber could be correctly interpreted. In addition, some accidental tracks could be eliminated because it was obvious they did not come from the vertex formed by the other showers in the event.

Plano-convex Lucite field lenses of focal length 423-in. were mounted on the optical faces of the chambers. The field lenses focused light leaving the chambers parallel to the optic axis on the camera. The camera lens had a focal length of 75 mm and produced a demagnification from real space to the film of 138.

Four fiducials were mounted at the corners of the optical faces of the spark chambers to provide reference marks on the film for the film-to-space reconstruction. The light from a spark passed through a Lucite frame, a Lucite field lens, and was then reflected by from four to six mirrors on its way to the camera. The combination of these optically imperfect elements produced a not negligible distortion at the camera. To correct for these distortions, transparent Mylar grids were placed at the front and back of each optical view of the chambers and photographed. The locations of the grids with respect to the fiducials were known so that

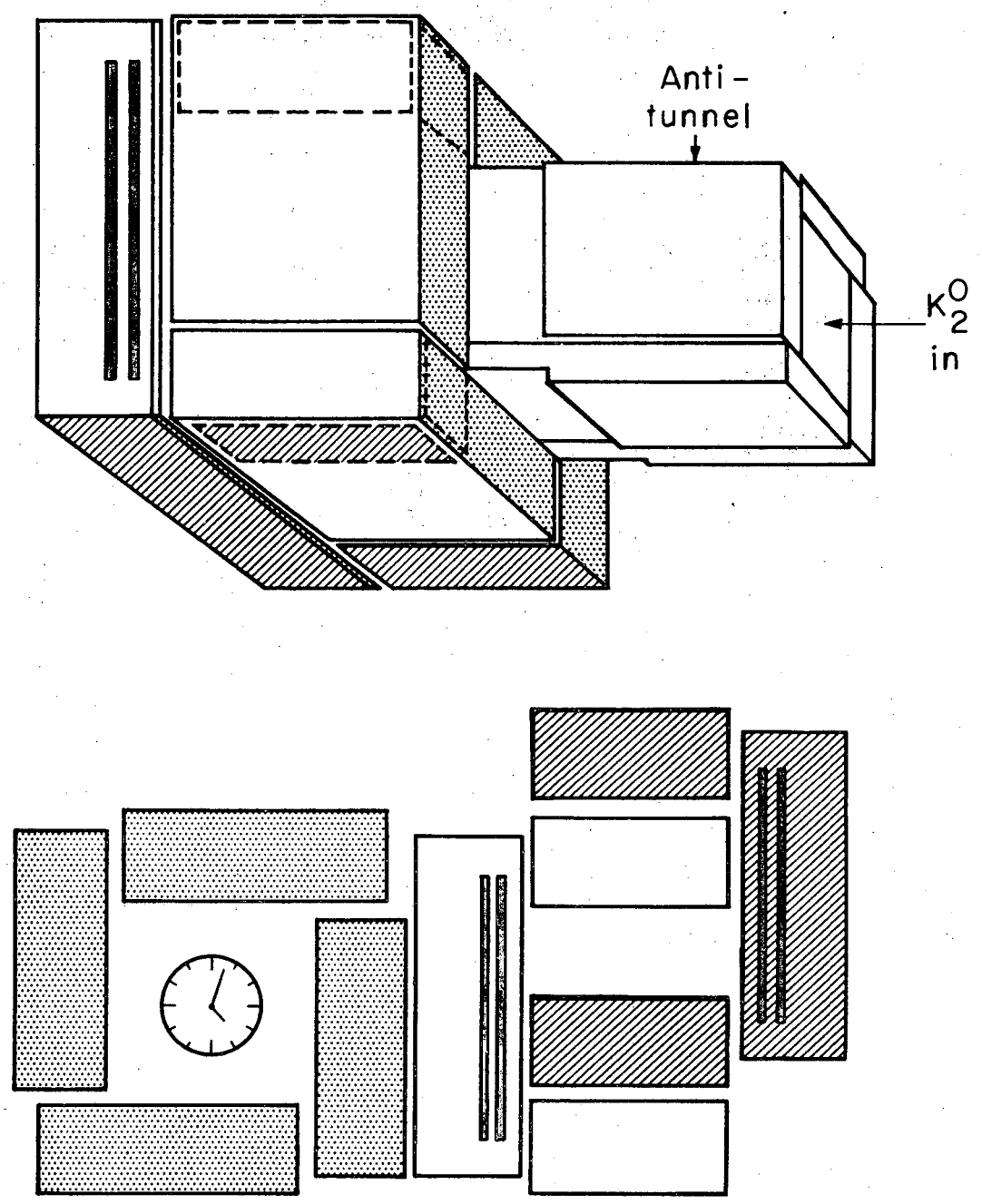

XBL681-1612

Fig. 5. (top) Perspective drawing of spark chamber array and gamma ray shower counter.

(bottom) Layout on film of views of spark chamber array. Shading indicates the correspondence between the views in the two drawings.

the mapping of real space onto the film was known for many discrete points distributed throughout the views. The space coordinates of the sparks were calculated by interpolation between known points on the grids. The distortions were usually less than 0.1 in. but in several bad areas became as great as 0.25 in.

E. Electronics

The flux of pions at the LH_2 target was monitored by two beam-defining, 8-in. diameter, 1/4-in. thick scintillation counters, M_1 and M_2, located at the exit of magnet Q_3 and at the entrance to the hydrogen target respectively. Pions which did not interact in the target were detected on their way to the beam dump by a similar third scintillation counter, M_3, located at the entrance to magnet B_4. Information about the pion momentum was obtained by monitoring the pion flux at the momentum-defining collimator at the entrance to magnet Q_2. Three scintillators, P_{1-3}, 3-in. high, 4-in. wide, and 1/4-in. thick divided the beam into three momentum bands, each with a momentum spread of approximately half that of the whole beam.

Gamma rays produced in the target by background reactions such as $\pi^- p \rightarrow \pi^o n$ and $\pi^- p \rightarrow \gamma n$ were filtered from the neutral beam by 4 in. of lead placed five feet downstream from the target. Four scintillation counters, L_{1-4}, were placed at depths of 1, 2.25, 3.25 and 4 in. in the lead. These counters were intended to veto events in which the shower was not completely contained but in which gamma rays escaped out the downstream side of the lead and traveled down to the spark chamber array. The electronic signature corresponding to the possible production of a K^o was taken to be $M_1 M_2 \bar{M}_3 \bar{L}_{1-4} = M$.

Since data were usually taken at beam fluxes of 10^7/sec, electronic circuitry capable of operating efficiently at high repetition rates was required. Most of the circuitry used was Chronetics 100 series nominally capable of repetition rates of 100 MH_z. The high rate also required that special precautions be taken with the beam counters. The current output required at the base for counters M_1, M_2, M_3, and L_{1-4} was reduced a factor

of 10 by introducing a wide-band, 1 nsec rise time, dc amplifier between the phototube output and the input to the Chronetics 101 discriminator.[17] Stable operation of the phototubes was further insured by the use of Zener diodes to provide the voltage for the last four stages of multiplication. Furthermore, 10 mas of additional current was supplied for the last two stages of multiplication.

The logic signals from M_3 and the L counters were combined in a deadtime-free fashion by means of a linear dc amplifier with multiple inputs. The sum was then used (through a dc couple) to veto the M_1M_2 coincidence. Hence the veto efficiency was kept high even though all anticounters were operating at high rates.

The rest of the circuitry was used to monitor the possible decay of a K_L^o. The signature for a decay into a neutral final state was taken to be (see Fig. 4): (1) no response from the A scintillation counters lining the inside walls of the spark chambers, (2) no response from the R scintillation counters embedded in the downstream chamber after the first aluminum gaps, and (3) response from at least two of the SC scintillator-Cerenkov trigger units separated by a minimum distance of two trigger units. The signature for (3) was obtained by taking the output of each trigger counter, splitting it into three signals, and then recombining these signals as shown in Fig. 6. The majority logic units require that a certain number of inputs be present without specifying any in particular.

The counts in the SC trigger units coincident with the above signature lit display lights mounted on the side of the downstream chamber directly over the ends of the corresponding counters. The trigger lights provided identification of low energy gamma ray showers which fired a trigger counter but produced only one or two sparks in the chamber. The

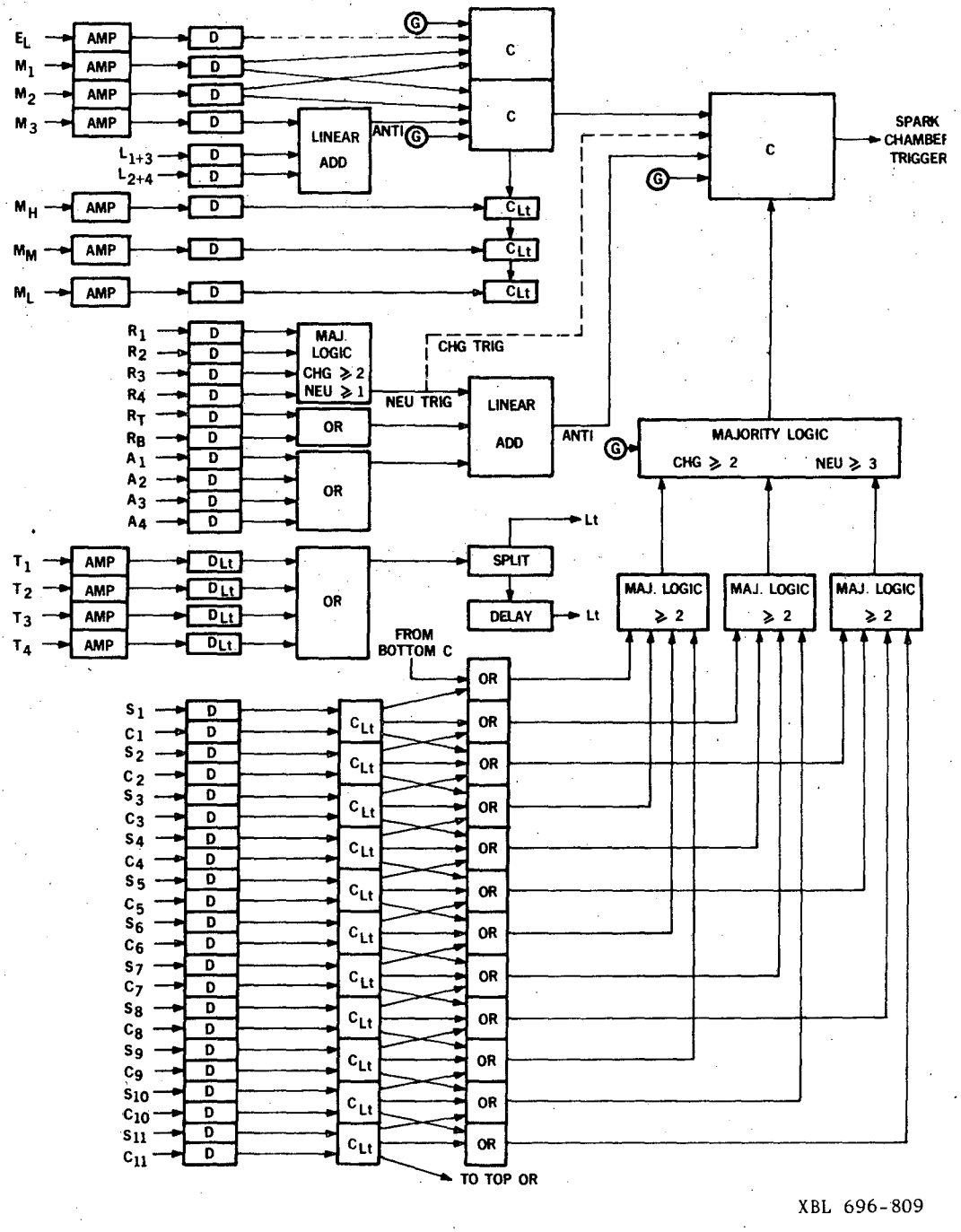

XBL 696-809

Fig. 6. Block diagram of fast electronics. Discriminators are denoted by the letter D; coincidence circuits by the letter C.

trigger lights were also used to discriminate against accidental tracks in the downstream chamber. Coincident counts in the entrance tunnel shower counters, T_{1-4}, as well as coincident counts in the momentum counters, P_{1-3}, were also recorded on the film by means of display lights.

The counters used in conjunction with the spark chambers had lengths of the order of 2 m with correspondingly large variations in light collection time. The variations were largest in the Lucite Cerenkov slabs due to the directional nature of emission of Cerenkov light and fluctuations due to the statistics of the low number of photons reaching the phototube. The jitter times of the SC pairs were reduced to nearly the jitter in the scintillator member alone by lengthening the Cerenkov discriminator output the extent of the maximum jitter and shifting it earlier. The timing of the pair was then determined by the arrival of the pulse from the scintillator member. The circuits combining the SC pairs had unavoidably broad resolution times (20 to 40 nsec) due to differences in the various particle and light collection paths. The accidental trigger rate was nevertheless fairly low. At maximum beam intensities the accidental rate was about 25%.

The signature for a charged final state was taken to be: (1) no response from the A scintillation counters, (2) no response from the top or bottom R counters, (3) response from two or more of the four inner R counters, and (4) response from two or more of the trigger scintillators separated by a minimum distance of one trigger unit. The charged signature could be obtained easily from the neutral signature by flipping 13 switches and changing one cable. Charged data taking was sandwiched in with the neutral runs and provided several systematic checks and calibrations of the experimental apparatus.

When the overall signature for the production and decay of a K_L^o was met the electronics was gated off and the spark chambers were fired. The picture-taking rate was limited by the time required for the HV supplies to recharge the pulsers (70 msec). The actual rate was one to two pictures/pulse for the neutral signature and five to six pictures/pulse for the charged signature. The sensitive time per Bevatron pulse was usually 600 to 800 msec.

Alternate plates of the spark chambers were charged up to high voltage by pulsers directly affixed to the plates. This low inductance connection made possible rise times of voltage on the plates of about 25 nsec. Each pulser had a capacitance of 15 000 pf and was used to drive a pair of gaps having a capacitance of 6000 pf. If no track was in the chamber the voltage was dumped by means of self-triggering spark gaps which were plugged into the chamber near critical points such as gas holes.[18] The duration of the pulse on the plates could be adjusted by varying the spacing of these gaps. For a peak voltage of 8 kV, 40 nsec FWHM was found to be the minimum pulse width which gave full multiple-track efficiency. For this width there were essentially no spurious breakdowns in the chambers.

The logic-level output generated by the electronics when the signature for an event was met fired a master pulser which drove in turn six slave gaps located at each of the chambers. The slave spark gaps then triggered the 23 to 26 pulsers used to fire each of the spark chambers. The total delay from the time an event occurred to the time the voltage appeared on the plates was about 350 nsec.

The spark chambers were operated with a dc clearing field of 20 volts. The debris of ions from the sparks was swept away by a pulsed, 40 msec,

150 volt clearing field applied during the recharging of the pulsers.

III. DATA ANALYSIS

A. Scanning

The initial stage in the data reduction process was the scanning of the film. The scanning served to provide a count of the total number of neutral decays of the K_L^o observed during the run and to select a subset of events which could possibly be $K_L^o \to 2\pi^o$ decays.

A neutral decay event was defined to be three or more gamma ray showers forming a vertex which could conceivably be in the decay volume. Random (with a weight proportional to the beam intensity) pulsing of the spark chambers under data-taking conditions showed only rarely the presence of spurious tracks. The results of the random-pulsing runs are summarized in Table I. In nearly all pictures there were at most only one or two

Table I. Results of scan of random-pulsing data.

Beam Intensity* Estimate (10^6)	Counted (10^6)	Tracks confusable with gamma ray shower. (%)	Counts in tunnel shower counter. (5)	All accidentals. (%)
13.3	10	3.6±0.6	4.5±0.5	11.6±1.1
26.2	15	9.5±1.5	8.6±1.4	22.9±2.4

*Flux of π, μ, and e during 700 msec spill. Data usually taken for counted intensities of 10×10^6 to 12×10^6. Estimated beam intensities were calculated from the rate of occurence of all accidentals using the assumptions that the observed accidentals rates are proportional to the beam intensity and that the counting efficiency of the beam monitor system decreases exponentially with beam intensity.

isolated single sparks. Thus it was possible to define a track as two or more sparks lined up in adjacent gaps. Showering tracks were easily distinguished from tracks due to heavy charged particles by their highly

scattered and disjointed nature. In all, the signature of three or more showers forming a vertex was so distinct that the presence of a K_L^o neutral decay could be unambiguously determined.

A run with the hydrogen target empty produced one neutral decay event during an interval in which 97 would have been seen with the target full. The expected number from the target end windows and the beam monitor scintillators was two.

Each roll of film was scanned twice. When an event was found, the scanners recorded the following information: frame number, total number of showers, total number of showers in the back spark chamber, the chamber numbers of any two-spark showers, the numbers of any tunnel shower counters fired, and the numbers of any P counters fired. The two scan lists were combined to form a master list of possible events. About 20% of the film was scanned a third time by physicists. This check scan showed the efficiency for at least one of the two scanners to record a K_L^o decay was greater than 99%.

The precise determination of the number of showers in an event was a more difficult problem. Since most of the separation of $2\pi^o$ decays from $3\pi^o$ decays occurred at the scanning table it was very important that this process be as free from error as possible. Each event on the combined list from the first two scans was examined by a physicist and a final judgement of the event was handed down. The events were categorized according to the number of showers present and the number of tunnel shower counters which were fired. In 92% of the events five or more gammas could be unambiguously identified. The four-shower events with no tunnel shower counts were candidates for $2\pi^o$ decays, and were divided into two classes: certain four showers and doubtful four showers. In the doubtful cases there was usually a fifth shower present which probably came from the decay point but

the possibility that it was produced by bremsstrahlung in one of the other showers could not be ruled out. The doubtful class comprised about 25% of the four-shower events. The distinction between these two classes of events was carried through the entire analysis. The failure of the doubtful class to produce any additional $2\pi^0$ decays constituted evidence for a selection efficiency for four-shower events of 100%. The selection efficiency was also checked by having another physicist perform a second selection. Comparison of the two selections indicated that the efficiency was about 98%.

B. Reconstruction

In order to normalize the $2\pi^o$ rate to the $3\pi^o$ rate it was necessary to apply the same fiducial volume cut to both types of events. Sample rolls of film were selected on which all frames showing a neutral K_L^o decay were measured. The fraction of events with decay points in the fiducial volume was calculated for each of the categories of data. These fractions were then applied to the total numbers of events found in the scanning for the different categories to estimate the total number of $3\pi^o$ decays in the fiducial volume.

The decay points used to determine the fiducial volume cuts were deduced from the directions of the gamma ray showers. The scattering of the electrons in the lead plates was great enough that only rarely did the shower preserve the direction of the gamma ray past the first few sparks. The events were measured on a film-plane digitizer. All the sparks in a shower were measured up to the point where the track first noticeably deviated from a straight line. The number of sparks usually measured in a shower was from three to five.

The decay point was then determined by the following procedure:

1. A straight line was fit through the measured sparks of each shower.
2. A trial decay point was analytically calculated which minimized the quantity

$$\sum_i g_i s_i^2$$

where s_i was the perpendicular distance from the decay point to the line drawn through the ith shower and g_i was the weighting factor for the ith shower. The showers were intially all given equal weights.

3. The distances, R_i, from the trial decay point to the beginning points of the showers were calculated.

4. The g_i were set equal to $1/R_i^2$ and a new decay point was calculated which now approximated a minimization of the rms value of the shower angular deviations.

5. Steps 3 and 4 were iterated four times, well past the point of convergence.

The final trial decay point was then taken as the initial point in a search routine which minimized a χ^2 constructed by summing in turn the squared lateral displacements of the measured sparks of each shower from a straight line drawn from the variable decay point through the first spark of that shower. The minimum in this χ^2 surface was taken as the best estimate of the decay point.

To prevent possible contamination of the data by $2\pi^o$ decays of K_S^o mesons regenerated in the tunnel shower counter or in the spark chamber plates, the boundaries of the fiducial volume were taken to be 2 in. away from any solid material. The 2-in. margin was safely greater than the usual uncertainty of 1/2 to 1 in. in the location of decay points for events close to the chambers. The fiducial volume was a rectangular prism with dimensions 40 by 40 in. perpendicular to the beam and 38 in. along the beam.

C. Spark Counting

The energy content of each shower was estimated by measuring the total apparent path length of the electrons in the lead plates. Tracings were made of the two views of the shower as it appeared on the scan table. The pattern of the shower was represented by a series of line segments drawn to follow the electrons as they scattered in the chamber plates. The line segments were drawn through corresponding parts of the shower in the two views. The line segments were then measured and a reconstructed real-space length calculated for each. The sum of the lengths was expressed as the number of equivalent sparks which would be visible for an electron traveling normally to the plates. Single isolated sparks could not be drawn as part of line segments but were counted and added to the equivalent spark total. Energy lost by the shower in traversing the trigger counters in the downstream chamber was also taken into account. The uncertainty in range for showers which did not pass all the way through a counter was reduced by using the information provided by the data lights which indicated whether or not the trigger counter had been fired.

The spark counting was calibrated using gamma rays of known energy from the π^o in $K_L^o \rightarrow \pi^+\pi^-\pi^o$ decay. The two charged pion tracks had much greater pointing accuracy than the gamma ray showers and were used alone to determine the decay point for the event. The directions of the charged pions and gamma rays were calculated from the location of the decay point and the locations of the points at which the tracks first appeared in the chambers. The direction of the incident K_L^o was also calculable since the location of its production point was well known. To the extent that the magnitude of the K_L^o momentum was known, the knowledge of the directions of the particles led to a kinematic one-constraint fit. The energies of

the charged pions and the two gamma rays were calculated using the three conservation-of-momentum equations and the invariant mass equation for the π^o. A self-consistency check was performed by calculating the total momentum of the four-particle system using the calculated energies and the conservation-of-energy equation. The calculated total momentum was required to be within 10% of the known K_L^o momentum. A plot of the spark counts versus the kinematically calculated energies is shown in Fig. 7. The spark counts on the average varied linearly with energy with a conversion constant of 5.0 MeV/equivalent spark. The percent error in the spark count was independent of energy and normally distributed with two-thirds of the spark counts within a factor of 1.5 of the kinematically determined energy. The spark count calibration was checked by applying the above counting techniques to six-shower events where all the energy of the K_L^o should be exhibited. The distribution of the total energy of the six showers as deduced by spark counting centered well with the known energy distribution of the K_L^o mesons. The comparison is shown in Fig. 8.

The analysis of the $K_L \rightarrow \pi^+\pi^-\pi^o$ events also provided a calibration of the pointing accuracy of the gamma rays as a function of energy. The directions of the showers were determined using the measuring techniques outlined above. The directions for the gamma rays deduced by drawing lines from the vertex formed by the π^+ and π^- tracks to the first sparks of the showers deviated from the shower directions as shown in Fig. 9.

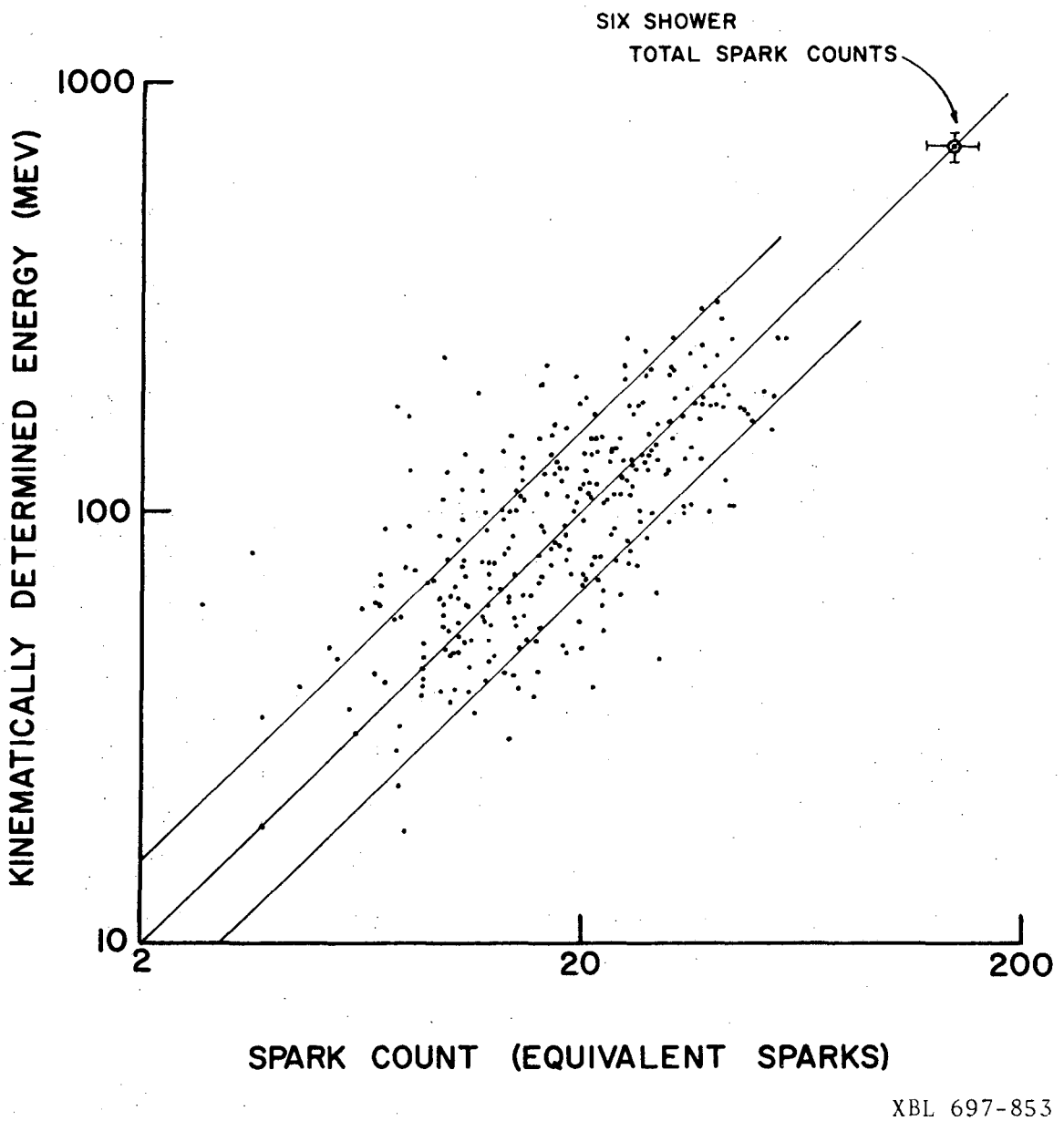

XBL 697-853

Fig. 7. Scatter plot of spark count vs. energy for gamma rays from the π^o in $K_L^o \to \pi^+\pi^-\pi^o$ decays. The central diagonal line represents a conversion constant of 5.0 MeV/eq. spark. The two adjacent diagonal lines enclose spark counts that are within a factor of 1.5 of the kinematically determined energy. This region contains two-thirds of the spark counts.

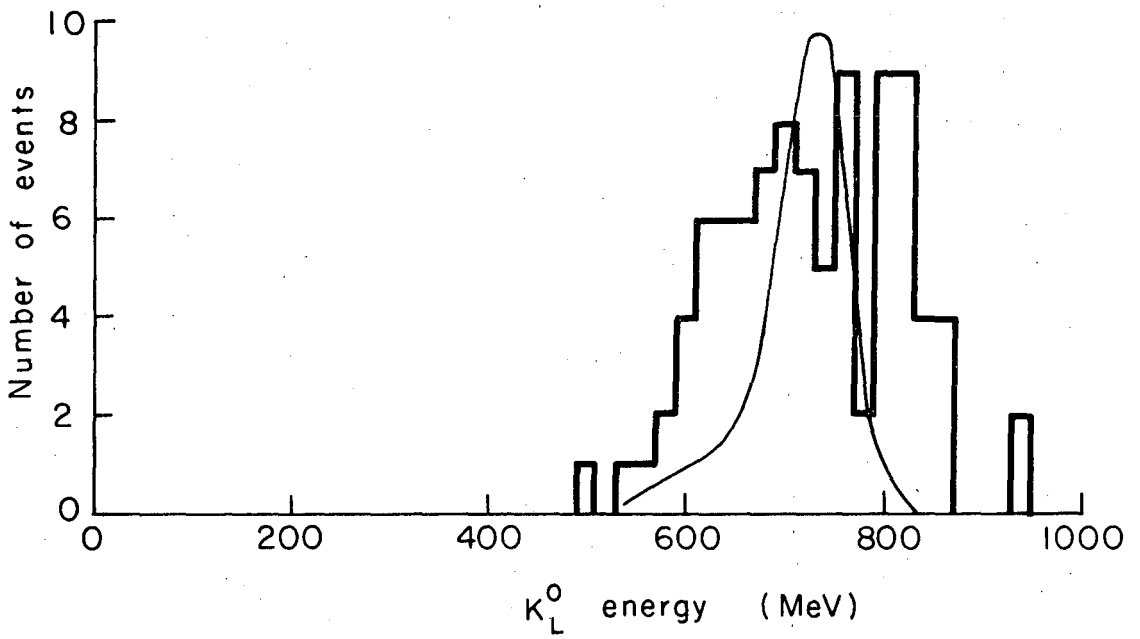

XBL695-2661

Fig. 8. Comparison of total spark counts for six-shower events (5 MeV/eq. spark) to the calculated energy spectrum of the K_L^0 beam as shown by smooth curve.

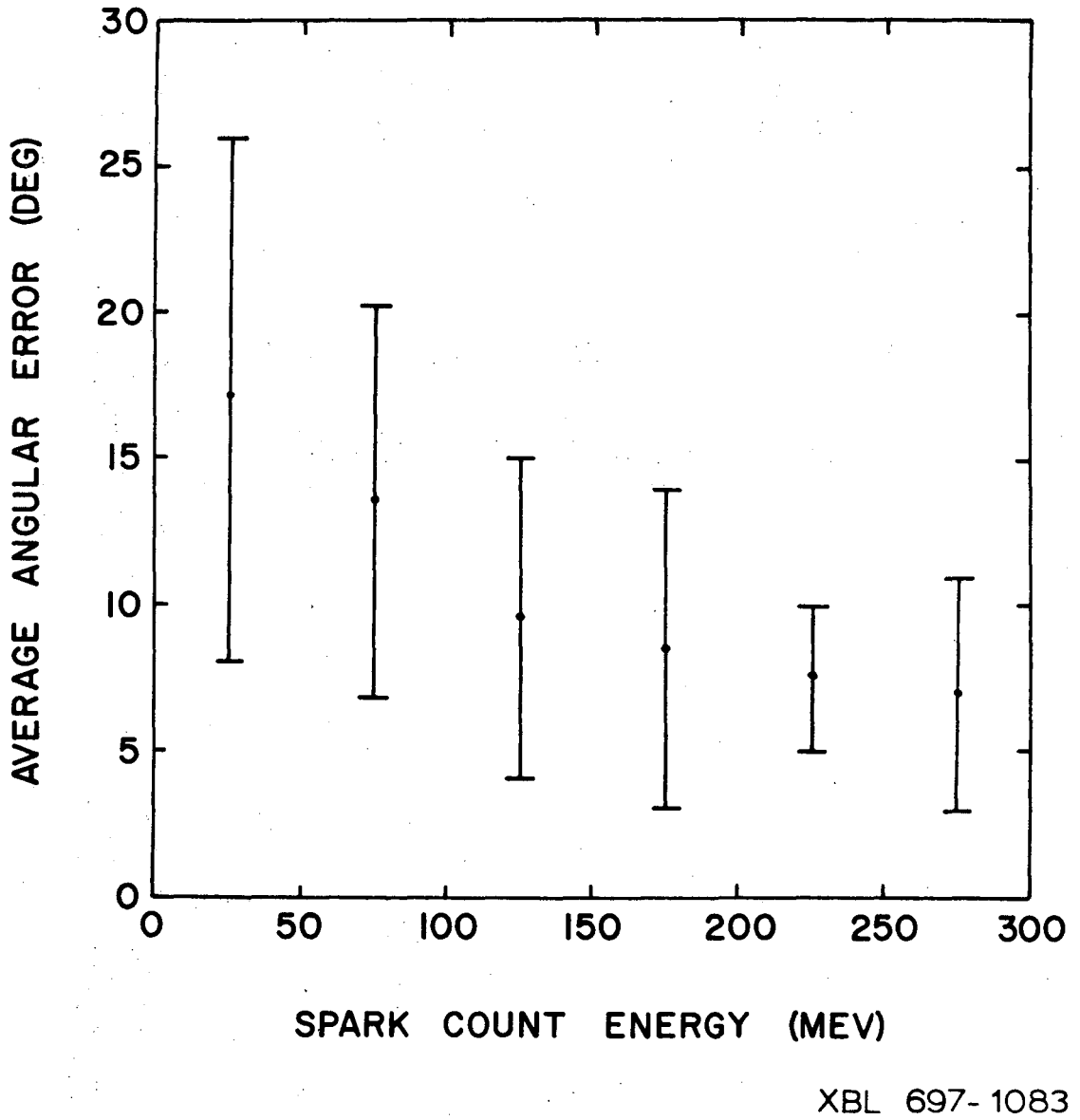

Fig. 9. Average angular error of gamma ray showers as a function of spark count energy as deduced from $K_L^o \rightarrow \pi^+\pi^-\pi^o$ calibration data. Bars enclose two-thirds of the showers in each energy bin.

D. Methods of Analysis

Two different methods were used to analyze the four-shower events for the presence of a $2\pi^o$ intermediate state. The two methods gave mutually consistent values for the number of $2\pi^o$ events in the data.

Method A. The vertex calculated from the directions of the four showers was taken to be the best estimate of the decay point. The directions of the gamma rays were calculated from the beginning points of the showers and the four-shower vertex. The direction of the incident K_L^o was calculated using the four-shower vertex and the known location of the K_L^o source. The gamma ray directions were then transformed into the rest frame of a 530 MeV/c K_L^o meson (the known mean momentum of the K_L^o beam) where the rest of the analysis proceeded.

In the K_L^o rest frame the pions in $K_L^o \rightarrow 2\pi^o$ decay are emitted in opposite directions with a momentum of 209 MeV/c. The opening angles between the gamma rays emitted from each π^o have a distribution which peaks sharply at a minimum value of 66 deg. The resolution of the experimental apparatus was folded into the theoretical distribution to produce a curve, $P(\theta)$, which represented the relative probabilities for various opening angles to be observed in a $2\pi^o$ decay. A product probability, $W(\theta_1,\theta_2) = P(\theta_1)P(\theta_2)$, was calculated for each of the three possible pairings of the gamma rays. The pairing with the maximum probability was selected for further analysis. The efficiency for selecting the correct pairing was 92% for Monte Carlo-generated $2\pi^o$ decays. The energies of the gamma rays were calculated from the equations of conservation of energy and momentum for the process $K_L^o \rightarrow 4\gamma$. The direction of each pion is determined, up to a two-fold ambiguity, by the assumed pion momentum and the opening angle of the 2γ decay. For an opening angle

ϕ, and pion velocity β, conservation of energy and momentum requires that the pion direction be in the plane of the gamma rays and be at an angle, α, to the bisector of the opening angle where α satisfies the equation

$$\cos(\alpha) = \frac{1}{\beta} \cos\ (\phi/2).$$

The π^o direction closer to the higher energy gamma ray was chosen. This choice is correct in the limit of no experimental errors. Finally, the cosine of the opening angle $\theta_{\pi\pi}$ between the two reconstructed pion directions was calculated. Distributions of the values of cos $(\theta_{\pi\pi})$ for two different cuts in $W(\theta_1, \theta_2)$ are shown in Fig. 10. The requirement of $W(\theta_1, \theta_2) > 0.2$ applied to Monte Carlo-generated events rejected 86% of the $3\pi^o$ decays and 44% of the $2\pi^o$ decays.

Method B. Method A tested the four-shower data for consistency with the hypothesis of a $2\pi^o$ decay of a 530 MeV/c K_L^o meson of known direction. Since the K_L^o momentum distribution had a width of $\pm$10%, the values of cos $\theta_{\pi\pi}$ calculated for actual $2\pi^o$ decays would be necessarily slightly shifted from the minimum value of -1 even if the decay point were known precisely. The reliance on the assumption of a K_L^o momentum and mass was avoidable, however. In Method B the four-shower events were tested only for consistency with the hypothesis of a $2\pi^o$ decay of a particle of known direction. The kinematics of the four-gamma system is completely determined if the four gamma ray directions and energies are known. The particle directions were calculable from the location of the decay point. The knowledge of the direction of the incident particle enabled one to write down two equations of conservation of transverse momentum for the four-gamma system. The hypothesis of a $2\pi^o$ intermediate state provided two additional kinematic constraints in the form of invariant mass equations

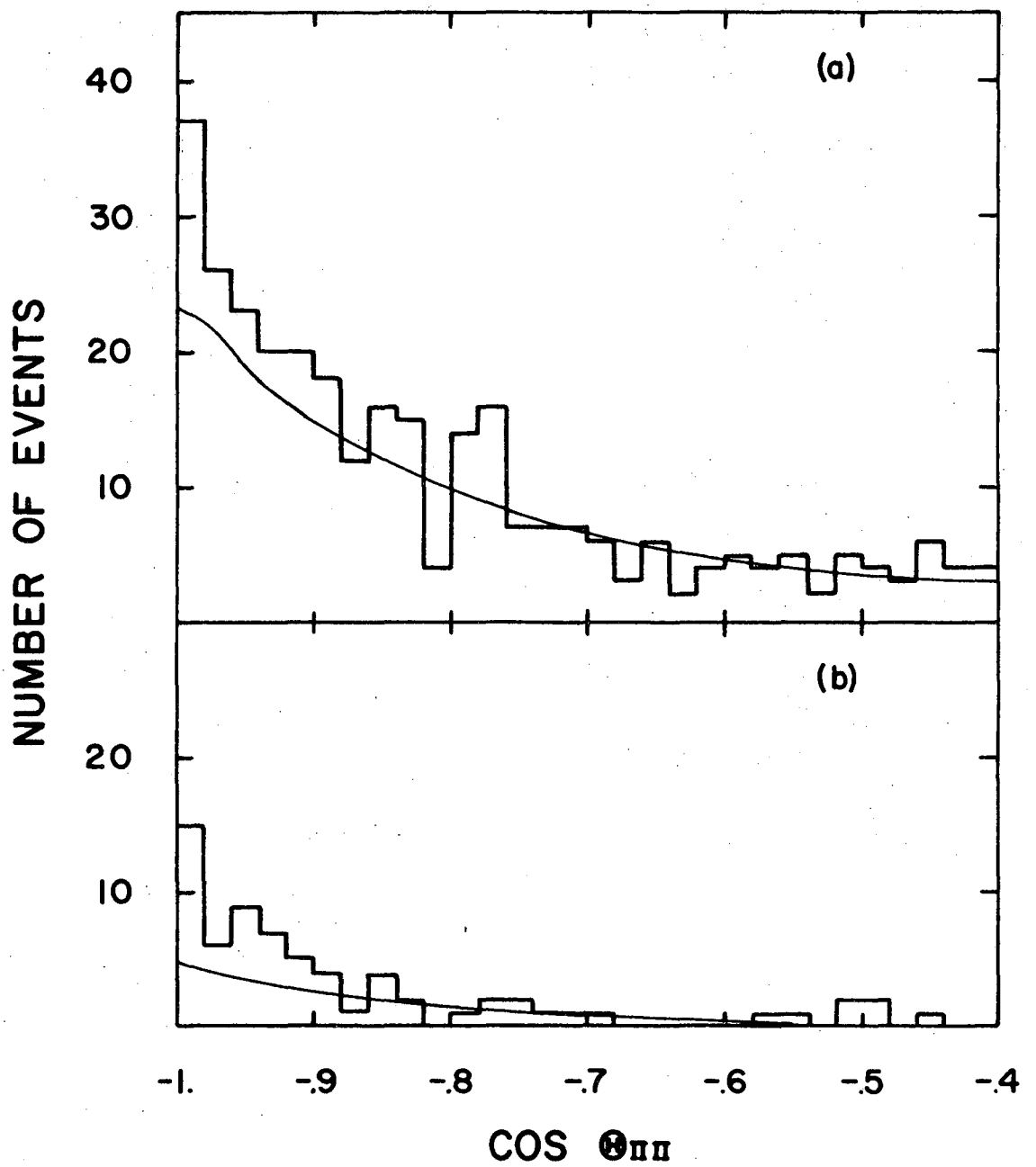

XBL 6911-6555

Fig. 10. Distribution in $\cos_{\pi\pi}$ for (a) all events, and (b) all events with $W(\theta_1, \theta_2) > 0.2$. Solid lines show Monte Carlo fits for the $3\pi^0$ background added to the background expected from the air.

for the two pairs of gamma rays. These four constraints determined the energies of the four gamma rays up to at most a six fold ambiguity: For a given pairing of the gamma rays, the four equations could be rewritten to produce a quadratic form in the square of any one of the gamma ray energies, hence for each of the three pairings there were at most two physically realizable solutions having all four gamma ray energies greater than zero. The solution of these equations is discussed in detail in Appendix A.

The errors in the experimental determination of the particle directions were largely due to the uncertainty in the location of the decay point. The locations of the source of the K_L^o mesons and the beginning points of the showers were all known with relatively high precision. If the exact decay point for a $2\pi^o$ decay were used in Method B one of the kinematic solutions for the four-gamma system would correspond almost exactly to a particle of the K_L^o mass with a momentum within the range known for the experiment. The spark count information was introduced in this method in an effort to improve the determination of the decay point.

A search operation was performed in which the decay point was allowed to vary until the best overall fit for the $2\pi^o$ hypothesis to the shower directions and spark count energies was obtained. The search operation was carried out for each of the physically realizable kinematic solutions. Seven different points were used as initial points in the search routine. One of these points was the decay point deduced from the shower directions alone which was used in Method A. The others were obtained from this point by going away a distance $\pm$ S along each of the coordinate axes. The distance S was the root-mean-square value for the distances of closest

approach to the decay point of lines fit through the different showers. If four positive energies could not be found at an initial point, no further search was made for this particular solution at this point.

The fitting parameters for the spark count energy information and the gamma shower angular information were constructed with the aid of the shower calibration data obtained from the $K_L^o \rightarrow \pi^+\pi^-\pi^o$ events. The $\pi^+\pi^-\pi^o$ decays provided data for gamma ray energies up to about 300 MeV. However the $2\pi^o$ decay of a K_L^o meson with momentum in the range known for the experiment can produce gamma rays with energies up to about 500 MeV. Hence it was necessary to make extrapolations of the calibration data. The spark count scatter plot (Fig. 7) showed that the errors in the spark counts were independent of energy with two-thirds of the spark counts within a factor of 1.5 of the kinematically determined energy. It was assumed that the errors were distributed in the same fashion for gamma ray energies up to 500 MeV. The fitting parameter for the spark count information was taken to be

$$\chi_E^2 = \sum_i \frac{\left[\ell n(EK_i/ES_i)\right]^2}{\left[\ell n(1.5)\right]^2}$$

where EK_i and ES_i were the kinematically calculated energy and spark count energy for the ith gamma ray. The factor of $1/\ell n(1.5)^2$ was introduced so that the average contribution to χ_E^2 for a shower in a $2\pi^o$ event would be about one.

The fitting parameter for the shower angular information was taken to be

$$\chi_A^2 = \sum_i \frac{(\Delta\theta_i)^2}{D_\theta^2(ES_i)}$$

where $\Delta\theta_i$ was the apparent angular deviation of the ith shower and

$D_\theta(ES_i)$ was the average error in angle for showers of spark count energy ES_i. For spark counts up to 300 MeV the values of D_θ were obtained from the $\pi^+\pi^-\pi^o$ data. The values of D_θ for spark counts between 300 and 500 MeV were obtained by linearly extrapolating the value of 6.0 deg at 300 MeV to a value of 4.0 deg at 500 MeV. The contribution of each shower to χ^2_A should on the average be roughly one. The use of the $1/\left[\ell n(1.5)\right]^2$ and $1/D_\theta^2$ factors was intended primarily to give the correct relative weighting to the spark count and shower angular information for use in the search program. No interpretation of the absolute values of the χ^2's has been made.

After the ≤ 42 search operations (seven initial points times three pairings times ≤ 2 solutions per pairing) had been carried out, the minimum point with the lowest value for the sum $\chi^2 = \chi^2_A + \chi^2_E$ was chosen to be the decay point. The gamma ray energies given by the solution corresponding to this pairing and decay point were used to calculate the total four-vector for the four-gamma system. The distribution of invariant mass values, M, for total momenta, P, between 430 MeV/c and 630 MeV/c is shown in Fig. 11.

If four positive energies were found at an initial point for a given pairing and solution then four positive energies could generally be found for most of the other initial points. The search program was almost always able to find the minimum point starting from any of these initial points. Analysis of Monte Carlo-generated $2\pi^o$ events showed that the efficiency of the search program to find a momentum value between 430 MeV/c and 630 MeV/c and a mass value greater than 430 MeV was 68%.

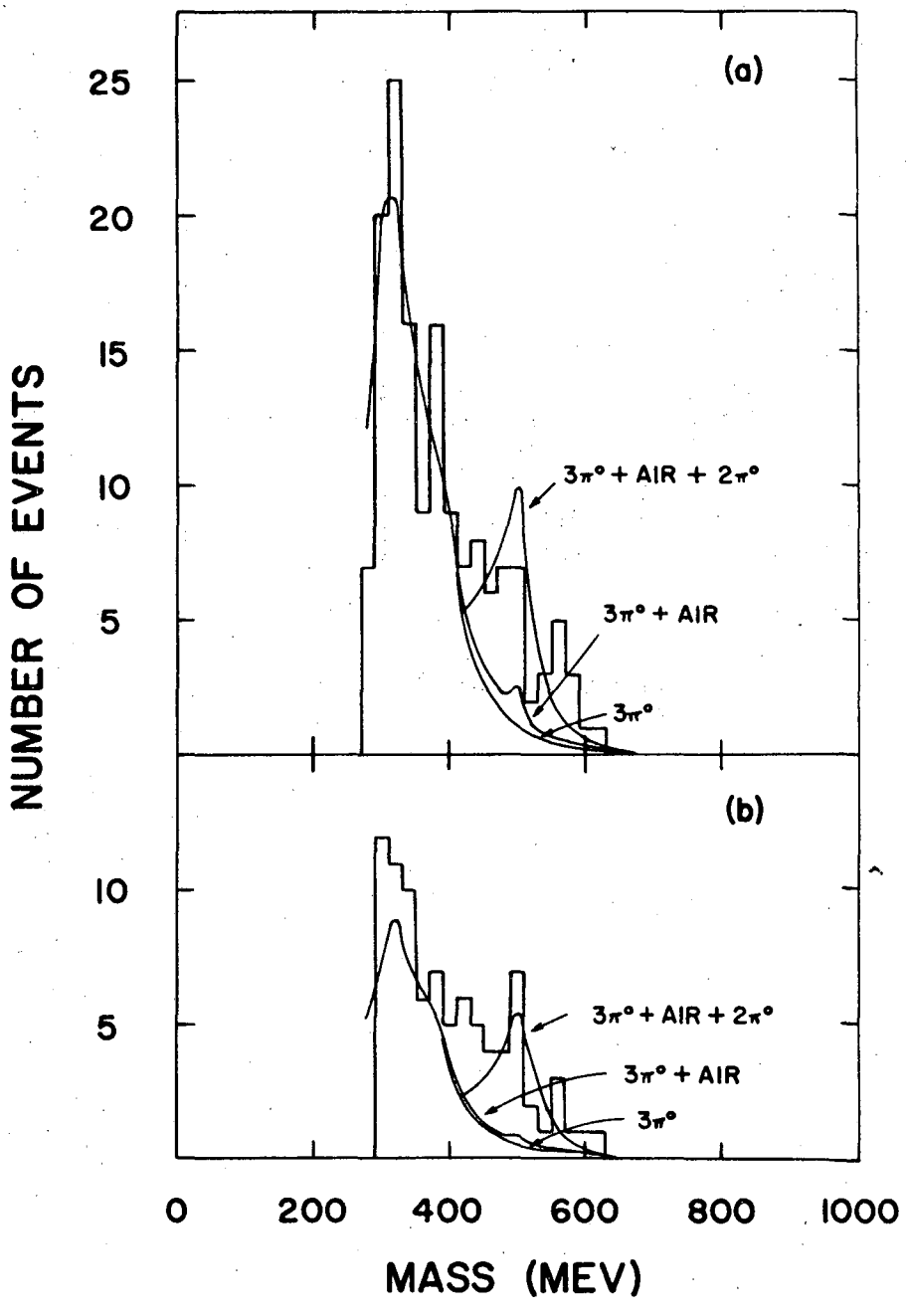

XBL 6911-6554

Fig. 11. Mass distributions for (a) all events with 430 MeV/c $\leq$ P $\leq$ 630 MeV/c, and (b) events from (a) also having $\chi^2 < 6.25$.

E. Monte Carlo Program

The calculation of the number of $2\pi^o$ events present in the four-shower data required knowledge of the behavior of both $2\pi^o$ and $3\pi^o$ events under the two different methods of analysis. A Monte Carlo computer program was written to simulate the appearance of $2\pi^o$ and $3\pi^o$ events in the experimental apparatus.

K_L^o mesons with the known momentum distribution for the experiment were generated and allowed to decay in a region which extended beyond the fiducial volume 3 in. downstream, 6 in. upstream, and 2 in. laterally. The decay of the K_L^o into pions was generated in the K_L^o barycentric system. The $3\pi^o$ decays were uniformly distributed over three-body phase space. The plane containing the three pion momentum vectors was randomly oriented in space. The pions in $2\pi^o$ decay were generated with equal and oppositely directed momenta of 209 MeV/c. The axis of the decay was randomly oriented in space. The four-vectors for the gamma rays from the $\pi^o \rightarrow 2\gamma$ decays were generated in the pion rest frames. The decay axes were randomly oriented in the pion rest frames. The gamma ray four-vectors were then transformed into the K_L^o barycentric system. Finally, all the gamma ray four-vectors were transformed into the lab system.

The conversion points of gamma rays which entered the spark chambers were determined from Compton and pair-creation cross sections.[19] The showers were generated from a library of case histories of the shower pointing accuracy, spark count, and geometric structure of gamma rays of known energy obtained from the $K_L^o \rightarrow \pi^+\pi^-\pi^o$ calibration data. The shower information for each gamma ray was kept together and binned in an energy interval. The Monte Carlo program used the library by going to the appropriate energy interval and finding a shower via a random table look-up.

The shower patterns were overlaid upon the real geometry of the spark chamber array to allow for efficiency losses due to purely structural features. The overlays were also used to determine whether or not an event would register in the appropriate combination of scintillator-Cerenkov trigger counters to generate a chamber trigger pulse. The shower library was supplemented at the low (< 25 MeV) and high (> 220 MeV) energy ends by synthetic events whose shower structure, spark counts, and angular errors were deduced by extrapolation from the existing library.

The Monte Carlo events were reconstructed from the gamma ray showers in the same manner as the experimental data. Comparisons of Monte Carlo events to data were made only for events whose reconstructed decay points were in the fiducial volume. Use of the shower library freed the Monte Carlo program from any reliance on an adjustable efficiency function for the spark chambers. Consequently Monte Carlo predictions for various experimental distributions dependent only on the properties of the chambers became rigorous checks of the validity of the program. The Monte Carlo program correctly predicted the observed distribution of gamma ray conversion points, the distribution of shower angular deviations from the deduced decay points, and the multiplicities of showers present in the chambers. The observed shower multiplicities (for all neutral decays with or without tunnel shower counts) were: 7: 3%, 6: 44%, 5: 35%, 4: 14%, 3: 4%. Use of the 7:6 ratio to correct the above percentages for accidental tracks gave: 6: 45%, 5: 36%, 4: 15%, 3: 4%. The Monte Carlo predictions for $3\pi^o$ events were: 6: 48%, 5: 39%, 4: 11%, 3: 1%.

In order to normalize the observed $2\pi^o$ rate to the $3\pi^o$ background, the Monte Carlo program was used to calculate the probability for a $3\pi^o$ decay to trigger and produce three or more showers in the spark chambers

and the probability for a $2\pi^0$ decay to trigger and give four showers. Observe that the tunnel shower counter is not used to detect either $2\pi^0$ or $3\pi^0$ decays. The calculation of the relative rates for $2\pi^0$ and $3\pi^0$ decay depended only on the ratio of these two detection efficiencies. This ratio was little changed by refinements made during the historical development of the Monte Carlo program. It was also little affected by variations deliberately introduced to test its sensitivity.

The Monte Carlo program used an efficiency function for the tunnel shower counter calculated from pair-creation and Compton cross-sections. The tunnel counter was important in improving the statistical accuracy of the experiment by reducing the confusable $3\pi^0$ background with four showers appearing in the spark chambers. However, the calculation of the $2\pi^0$ rate was insensitive to its assumed efficiency. The tunnel counter did not enter into the calculation of detection efficiencies for either $3\pi^0$ or $2\pi^0$ decay. Its only possible influence was through its effect on the shape of the $3\pi^0$ background which produced four showers in the spark chambers and no tunnel shower counts. Monte Carlo $3\pi^0$ events with four visible showers and one tunnel shower count were analyzed and found to have nearly the same shape as four-shower $3\pi^0$ events with no tunnel shower counts. Hence the overall effect of the assumed tunnel efficiency on the calculation of the $2\pi^0$ rate was completely negligible.

The efficiency of the Cerenkov trigger counters had been measured to be 95 to 97% for minimum-ionizing particles at normal incidence which traverse the full 1.5-in. thickness of Lucite. Similar measurements for Lucite slabs 1-in. and 1/2-in. thick were also made and gave efficiencies of 93 and 71% respectively. The efficiency of the Cerenkov counters was taken to be zero for path lengths in the counter less than 0.1-in. and

was increased linearly until an efficiency of one was reached for a path length of 1.1 in. Tests were made with two variant efficiency functions: the first was zero for zero path length and increased linearly until an efficiency of one was reached at 0.5 in.; the second was zero for path lengths below 0.4 in. and increased linearly until an efficiency of one was reached at 1.4 in. The variation in the calculated relative detection efficiencies for $2\pi^o$ and $3\pi^o$ decays was less than 5%.

F. Results

The number of $2\pi^o$ decays in the four-shower data was calculated with a maximum-likelihood program which fit the experimental data with a superposition of $2\pi^o$ and $3\pi^o$ Monte Carlo distributions in the relevant variables (Method A: $W(\theta_1, \theta_2)$ and $\cos\theta_{\pi\pi}$; Method B: P, M, and χ^2).

Before the fit to the $2\pi^o$ and $3\pi^o$ distributions was made, the four-shower events were corrected for background generated in the air-filled decay volume. The correction was deduced from data taken with the decay volume filled with beryllium. Five Be slabs, 36-in. wide by 35-in. high by 1-in. thick, were spaced at 5-in. intervals in the central part of the decay volume. The same triggering requirements were used for the Be as for the air data.

The normalization of the Be data to the air data was obtained through the pion beam monitor counters. The number of neutral decays in air per beam monitor count was known for the beam conditions under which the Be data were taken. The number of Be events could then be normalized to the total number of K_L^o neutral decays in air.

The Monte Carlo program was used to calculate a correction for the effect of the greater gamma absorption in Be. The average probability for all four gamma rays in a regenerated $K_S^o \to 2\pi^o$ decay to escape from the Be was calculated to be 0.67. The number of Be four-shower events was corrected by the factor 1/0.67. The contribution to the four-shower category of $K_L^o \to 3\pi^o$ decays in the Be was negligible since the A counters detected the showers emerging from the Be and vetoed these events.

The expected number of four-shower events due to the air was then calculated from the number observed in Be using the assumption that the cross-sections producing the background are proportional to atomic weight.

The Be four-shower events were analyzed in the same manner as the air data. The distributions produced were corrected for the change from Be to air and subtracted directly from the distributions obtained for the air data. The correction for the air background resulted in a 10% reduction in the calculated number of $K_L^o \rightarrow 2\pi^o$ decays present in the four-shower data.

The number of $K_L^o \rightarrow 2\pi^o$ decays in the four-shower data was calculated to be $\eta_2 = 40 \pm 11$ for Method A and $\eta_2 = 42 \pm 8$ for Method B. The likelihood function was found to be Gaussian about its maximum for both methods. The quoted error is taken at the $e^{-0.5}$ points. For Method A, the data were fit over the entire range of the variables $W(\theta_1, \theta_2)$ and $\cos(\theta_{\pi\pi})$. For Method B, the fit was made over the entire ranges of M and χ^2 but with the values of P restricted to the region 430 MeV/c to 630 MeV/c. The fits of the Monte Carlo distributions to the data are shown in Figs. 10 and 11. The results of Method B indicate that in the region $M > 430$ MeV (for all χ^2) the ratio of $2\pi^o$ decays to $3\pi^o$ decays is 0.96. Application of the momentum requirement $430 \text{ MeV/c} < P < 630 \text{ MeV/c}$ improves this ratio to 1.80.

The Monte Carlo prediction for the shape of the $3\pi^o$ four-shower background was checked by analyzing a sample of five-shower events as four-shower events. The shower with the lowest spark count was discarded and the remaining four showers analyzed under Method B to produce the mass distributions shown in Fig. 12. The mass distributions are fit well by the Monte Carlo predictions for five-shower events treated in this fashion (as also shown in Fig. 12). The mass distributions for Monte Carlo four-shower events and Monte Carlo five-shower (minus the lowest spark-count shower) events are nearly identical. Since the five-shower prediction

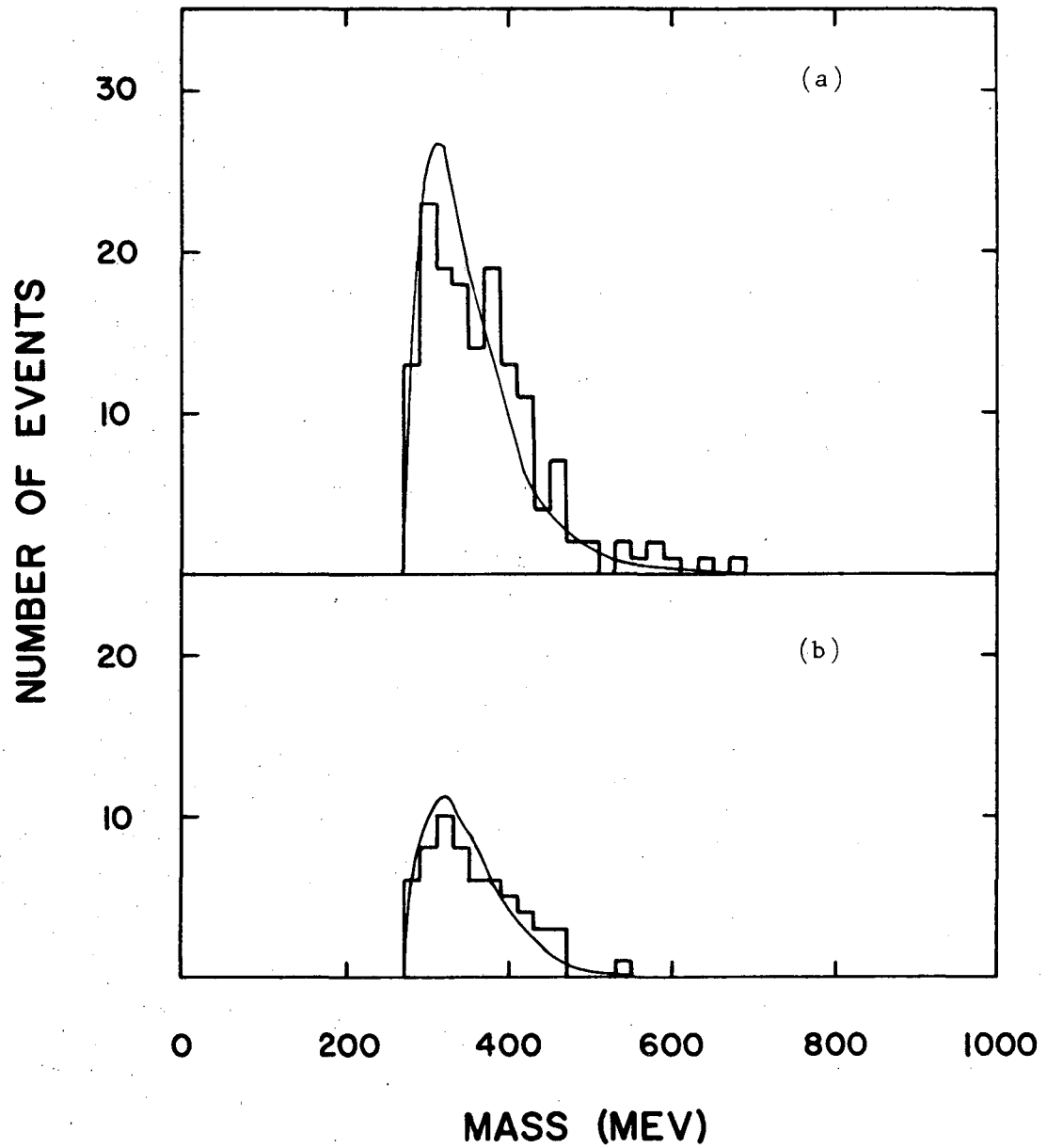

XBL 6911-6556

Fig. 12. Mass distributions for a sample of five-shower events analyzed as four showers by discarding the shower with the lowest spark count for (a) all events, and (b) all events having $\chi^2 < 6.25$. Solid lines are the Monte Carlo fits to the data.

fits the data well presumably the four-shower prediction fits well also.

A systematic correction of $1.09\pm.01$ for loss of events due to a fifth accidental shower or an accidental tunnel count was made to η_2. A systematic error of ± 4 events was assigned to η_2 to account for differences between Methods A and B and the experimental uncertainty in the spark count calibration and size of angular errors. The final value for the number of $2\pi^o$ four-shower events in the data was $\eta_2 = 45\pm 8$ (stat.) $\pm$ 4 (syst.).

The ratio of the rates

$$R = \frac{\Gamma(K_L \to 2\pi^o)}{\Gamma(K_L \to 3\pi^o)}$$

was calculated from η_2 using the equation $R = \left(\frac{t_3}{t_2 S_2}\right) \times (\eta_2/\eta_3)$ where η_3 was the total number of $3\pi^o$ decays observed and t_3/t_2S_2 = (probability for a $3\pi^o$ to trigger)/(probability for a $2\pi^o$ trigger and give four showers). The Monte Carlo program gave $t_3/t_2S_2 = 0.219/(0.156 \times 0.715) = 1.96\pm.01$. The result for the branching ratio is $R = 1.96(45/8773) = .0100\pm.0018$ (stat.) $\pm.0009$ (syst.). This result is based only on the fraction (40%) of the data which was analyzed at the Lawrence Radiation Laboratory in the manner described in this paper. A preliminary result based on all the data is $R = 0.0131\pm0.0018$ (stat.) $\pm$ .0025 (syst.).[20] The LRL fraction gave a relatively smaller statistical error because it was fit better by the Monte Carlo predictions. The improvement in systematic error was primarily the result of lack of uncertainty due to poorly known scanning efficiency.

IV. CONCLUSIONS

The value for the branching ratio $R = \frac{\Gamma(K_L \to 2\pi^o)}{\Gamma(K_L \to 3\pi^o)}$ obtained here leads to a value for $R_L = \frac{\Gamma(K_L \to 2\pi^o)}{\Gamma(K_L \to \pi^+\pi^-)}$ of $1.37 \pm .25$ (stat.) $\pm$ .14 (syst.). The systematic error in R_L was increased by 0.01 to account for the uncertainty in the values of the branching ratios $\frac{R(K_L \to 3\pi^o)}{R(K_L \to \text{all})}$ and $\frac{R(K_L \to \pi^+\pi^-)}{R(K_L \to \text{all})}$ used in the calculation.[21] The value of the ratio $R_S = \frac{\Gamma(K_S \to 2\pi^o)}{\Gamma(K_S \to \pi^+\pi^-)}$ is $0.462 \pm .018$.[21] The significant difference between R_L and R_S shows that CP is not conserved in the $K^o \to 2\pi$ decay process.

In the parameterization of the neutral K system used by Lee and Wu[5] (which is a slight modification of a parameterization introduced by Wu and Yang[22]) the K_L^o and K_S^o states are written

$$|K_S^o\rangle = \frac{1}{\left[2(1 + |\epsilon|^2)\right]^{1/2}}\left[(1 + \epsilon)|K^o\rangle + (1 - \epsilon)\,|K^o\rangle\right]$$

$$|K_L^o\rangle = \frac{1}{\left[2(1 + |\epsilon|^2)\right]^{1/2}}\left[(1 + \epsilon)\,|K^o\rangle - (1 - \epsilon)|\bar{K}^o\rangle\right]$$

where ϵ is a complex number and CPT invariance has been assumed. The relative phase between the $|K^o\rangle$ and $|\bar{K}^o\rangle$ is chosen implicitly such that the decay amplitude for $K_o \to (2\pi)_{I=0}$ can be written $A_o e^{i\delta_o}$ where A_o is real and δ_o is the π-π S-wave, I = 0, scattering phase shift at the energy of the K^o rest mass.

The dominance of $\Delta I = 1/2$ amplitudes in $K \to \pi + \pi$ decay $\left(\frac{A_2}{A_0} \ll 1\right)$ as well as the experimentally observed small value for $\frac{\Gamma(K_L \to \pi^+\pi^-)}{\Gamma(K_S \to \pi^+\pi^-)}$ imply that $\epsilon \ll 1$.[22] Two parameters directly related to

experimentally observable quantities are

$$\eta_{+-} = \frac{<\pi^+\pi^-|H_w|K_L^o>}{<\pi^+\pi^-|H_w|K_S^o>}$$

and $$\eta_{oo} = \frac{<\pi^o\pi^o|H_w|K_L^o>}{<\pi^o\pi^o|H_w|K_S^o>} .$$

To first-order in ϵ and $|A_2|/|A_0|$

$$\eta_{+-} = \epsilon + \epsilon'$$

and $$\eta_{oo} = \epsilon - 2\epsilon'$$

where

$$\epsilon' = \frac{i}{\sqrt{2}} \frac{\mathrm{Im}A_2}{A_o} e^{i(\delta_2 - \delta_0)} .$$

The value for $|\eta_{oo}|^2$ obtained using the results of this experiment is

$$|\eta_{oo}|^2 = 10.8 \pm 1.9 \text{ (stat.)} \pm 1 \text{ (syst.)} \times 10^{-6}.$$

Measurements of the ratio $\Gamma(K_L \to \pi^+\pi^-)/\Gamma(K_L \to \text{charged})$[6,9,10] give for $|\eta_{+-}|^2$ a value of

$$|\eta_{+-}|^2 = (3.69 \pm .15) \times 10^{-6}.$$

The difference between $|\eta_{+-}|^2$ and $|\eta_{oo}|^2$ corresponds to the difference between R_L and R_S noted earlier. In the parameterization of Wu and Yang it is seen that ϵ' (or Im A_2) cannot be equal to zero. The difference in phase between A_0 and A_2 indicates that CP is violated in the transition amplitudes for $K^o \to 2\pi$ decay.

ACKNOWLEDGEMENTS

The interest and support of Professor A. Carl Helmholz and Professor Burton J. Moyer, especially during the darkest hours of the experiment, is appreciated.

Professor Sherwood Parker contributed centrally to the idea of the experiment, the design of apparatus, and the maintenance of good experimental technique during the run.

Dr. Charles Rey was the principal designer of the spark chambers, the mirror system, and the electronics required to pulse the chambers. The outstanding performance of the spark chambers is largely the result of his efforts.

Tim Daly scanned with uniform excellence 600 000 frames of the film, measured 7000 events of interest, and drew several of the figures appearing in this thesis. His efforts are greatly appreciated.

Garth Burns scanned all the $K_L^o \to \pi^+\pi^-\pi^o$ calibration data. Paul Meilleur drew most of the shower pattern tracings. I thank them both for their large contributions of accurate work.

Michael Raugh was the principal author of the computer program which performed the film-to-real space transformations. He set up and supervised the difficult task of data acquisition required to put the information in the grid pictures into a usable form.

Emily Friedman pleasantly performed many checks of the state of the experimental apparatus during the course of the run.

I thank Carl Harrington and the other operators of the CDC 6600 computer for their generally speedy running of the hundreds of jobs required for the development of the analysis of the experiment.

Miss Miriam Machlis helped me put this thesis into good technical form and cheerfully typed several drafts of many of the sections. I

APPENDIX

A. Solution of Equations Used in Method B.

In the analysis of Method B the hypothesis of an intermediate $2\pi^o$ state was used to calculate the gamma ray energies from the experimentally determined directions of the K_L^o and the four gamma rays.

Consider a particle traveling along the z axis which decays into four gamma rays. The equations of conservation of transverse momentum are

$$\sum_{i=1}^{4} \alpha_i P_i = 0 \tag{1}$$

and

$$\sum_{i=1}^{4} \beta_i P_i = 0 \tag{2}$$

where α_i is the x direction cosine, β_i is the y direction cosine and P_i is the energy of the ith gamma ray.

To be specific, consider the pairing in which gamma rays 1 and 2 come from one π^o and 3 and 4 come from the other. The equations of invariant mass for the two-gamma systems are

$$P_1 P_2 = \frac{m_\pi^2}{2} \frac{1}{(1 - \cos \theta_{12})} \equiv d_{12} \tag{3}$$

and

$$P_3 P_4 = \frac{m_\pi^2}{2} \frac{1}{(1 - \cos \theta_{34})} \equiv d_{34} \tag{4}$$

where θ_{jk} is the angle between the jth and kth gamma rays and m_π is the π^o mass.

Equations (3) and (4) can be used to eliminate the variables P_2 and P_4 in Eqs. (1) and (2) to give

$$\alpha_1 P_1 + \alpha_2 \frac{d_{12}}{P_1} + \alpha_3 P_3 + \alpha_4 \frac{d_{34}}{P_3} = 0 \tag{5}$$

$$\beta_1 P_1 + \beta_2 \frac{d_{12}}{P_1} + \beta_3 P_3 + \beta_4 \frac{d_{34}}{P_3} = 0 . \qquad (6)$$

The linear combination of Eqs. (5) and (6) which does not contain a term proportional to $1/P_1$ is

$$P_1(\alpha_1\beta_2 - \alpha_2\beta_1) + P_3(\alpha_3\beta_2 - \alpha_2\beta_3) + \frac{d_{34}}{P_3}(\alpha_4\beta_2 - \alpha_2\beta_4) = 0 . \qquad (7)$$

The linear combination of Eqs. (5) and (6) which does not contain a term proportional to $1/P_3$ is

$$P_1(\alpha_1\beta_4 - \alpha_4\beta_1) + \frac{d_{12}}{P_1}(\alpha_2\beta_4 - \alpha_4\beta_2) + P_3(\alpha_3\beta_4 - \alpha_4\beta_3) = 0. \qquad (8)$$

If we introduce the notation

$$a_1 = \alpha_1\beta_2 - \alpha_2\beta_1 ,$$

$$b_1 = \alpha_1\beta_4 - \alpha_4\beta_1 ,$$

$$a_2 = \alpha_3\beta_2 - \alpha_2\beta_3 ,$$

$$b_2 = \alpha_2\beta_4 - \alpha_4\beta_2 ,$$

$$a_3 = (\alpha_4\beta_2 - \alpha_2\beta_4)d_{34} ,$$

and $$b_3 = (\alpha_3\beta_4 - \alpha_4\beta_3),$$

Eqs. (7) and (8) can be rewritten as

$$a_1 P_1 P_3 + a_2 P_3^2 + a_3 = 0 \qquad (9)$$

and $$b_1 P_1^2 + b_2 + b_3 P_1 P_3 = 0. \qquad (10)$$

Solution of Eq. (10) for P_3 in terms of P_1 gives

$$P_3 = \frac{-b_2 - b_1 P_1^2}{b_3 P_1} . \qquad (11)$$

Use of Eq. (11) to eliminate P_3 from Eq. (9) produces a quadratic form in P_1^2:

$$P_1^4\left[a_2b_1^2 - a_1b_1b_3\right] + P_1^2\left[a_3b_3^2 + 2a_2b_1b_2 - a_1b_2b_3\right] + a_2b_2^2 = 0. \quad (12)$$

There are at most two positive values of P_1 which are solutions of Eq. (12).

Equations (3), (4), and (11) provide only one solution for P_2, P_4 and P_3 for each solution for P_1; hence there are at most two sets of solutions with four positive energies for each of the possible gamma ray pairings.

REFERENCES

1. P. K. Kabir, The CP Puzzle, (Academic Press, London and New York, 1968).

2. M. V. Terent'ev, Usp. Fiz. Nauk 86, 231 (1965).

3. V. F. Weisskopf and E. P. Wigner, Z. Phys. 63, 54 and 65, 18 (1930).

4. G. Breit and I. S. Lowen, Phys. Rev. 46, 590 (1934).

5. T. D. Lee and C. S. Wu, A. Rev. Nucl. Sci. 16, 471 (1966).

6. J. H. Christenson, J. W. Cronin, V. L. Fitch, and R. Turlay, Phys. Rev. Letters 13, 138 (1964).

7. M. Levy and M. Nauenberg, Phys. Letters 12, 155 (1964).

8. V. L. Fitch, R. F. Roth, J. S. Russ, and W. Vernon, Phys. Rev. Letters 15, 73 (1965).

9. W. Galbraith, G. Manning, A. E. Taylor, B. D. Jones, J. Malos, A. Astbury, N. H. Lipman, and T. G. Walker, Phys. Rev. Letters 14, 383 (1965).

10. M. Bott-Bodenhausen, X. DeBouard, D. G. Cassel, D. Dekkers, R. Felst, R. Metmod, I. Savin, P. Scharff, M. Vivargent, T. R. Willitts and K. Winter, Phys. Letters 23, 277 (1966).

11. M. Banner, J. W. Cronin, J. K. Liu, and J. E. Pilcher, Phys. Rev. Letters 21, 1107 (1968).

12. I. A. Budagov, D. C. Cundy, G. Myatt, F. A. Nezrick, G. H. Trilling, W. Venus, H. Yoshiki, B. Aubert, P. Heusse, I. LeDong, J. P. Lowys, D. Moullet, E. Nagy, C. Pascaud, L. Behr, P. Beilliere, G. Boutang, M. Schiff, and J. Van Der Velde, Phys. Letters 28B, 215 (1968).

13. D. F. Bartlett, R. K. Carnegie, V. L. Fitch, K. Goulianos, D. P. Hutchinson, T. Kamae, R. F. Roth, J. S. Russ, and W. Vernon, Phys. Rev. Letters 21, 558 (1968).

14. J-M. Gaillard, W. Galbraith, A. Hussri, M. R. Jane, N. H. Lipman, G. Manning, T. Ratcliffe, H. Faissner, and H. Reithler, Nuovo Cimento 59A, 453 (1969).

15. L. Bertanza, P. L. Connolly, B. B. Culwick, F. R. Eisler, T. Morris, R. Palmer, A. Prodell, and N. P. Samios, Phys. Rev. Letters 8, 332 (1962).

16. L. B. Leipuner and R. K. Adair, Phys. Rev. 109, 1358 (1958).

17. H. G. Jackson and J. A. Mattis, IEEE Journal of Solid-state Circuits SC-4, 86 (1969).

18. C. A. Rey and S. I. Parker, Nucl. Instr. and Meth. 54, 314 (1967).

19. Gladys White Grodstein, X-Ray Attenuation Coefficients from 10 kev to 100 Mev, NBS Circular 583 (April 30, 1957).

20. R. J. Cence, B. D. Jones, V. Z. Peterson, V. J. Stenger, J. Wilson, D. Cheng, R. D. Eandi, R. W. Kenney, I. Linscott, W. P. Oliver, S. Parker, and C. Rey, Phys. Rev. Letters 22, 1210 (1969).

21. N. Barish-Schmidt, A. Barbaro-Galtieri, L. R. Price, A. H. Rosenfeld, P. Söding, C. G. Wohl, M. Roos, and G. Conforto, Rev. Mod. Phys. 41, 109 (1969).

22. Tai Tsun Wu and C. N. Yang, Phys. Rev. Letters 13, 380 (1964).

TECHNICAL INFORMATION DIVISION
LAWRENCE RADIATION LABORATORY
UNIVERSITY OF CALIFORNIA
BERKELEY, CALIFORNIA 94720